**Title:** The *Setaria viridis* genome and diversity panel enables discovery of a novel domestication gene

**Authors:** Sujan Mamidi[1,*], Adam Healey[1,*], Pu Huang[2,5,*]Jane Grimwood[1], Jerry Jenkins[1], Kerrie Barry[3], Avinash Sreedasyam[1], Shengqiang Shu[3], John T. Lovell[1], Maximilian Feldman[2,6], Jinxia Wu[1,7], Yunqing Yu[2], Cindy Chen[3], Jenifer Johnson[3], Hitoshi Sakakibara[4,8], Takatoshi Kiba[4,8], Tetsuya Sakurai[4,9], Rachel Tavares[2,10], Dmitri A. Nusinow[2], Ivan Baxter[2], Jeremy Schmutz[1,3], Thomas P. Brutnell[2,7], Elizabeth A. Kellogg[2,**]

[1] HudsonAlpha Institute for Biotechnology, Huntsville, Alabama, USA

[2] Donald Danforth Plant Science Center, 975 North Warson Road, St. Louis, MO 63132, USA

[3] Department of Energy Joint Genome Institute, Lawrence Berkeley National Laboratory, 1 Cyclotron Road, Berkeley, CA 94720, USA

[4] RIKEN Center for Sustainable Resource Science, Tsurumi, Yokohama 230-0045, Japan

[5] present address: BASF Corporation, 26 Davis Dr., Durham, NC 27709, USA

[6] present address: USDA-ARS Temperate Tree Fruit and Vegetable Research Unit, 24106 N. Bunn Rd., Prosser, WA 99350, USA

[7] Biotechnology Research Institute, Chinese Academy of Agricultural Sciences, Beijing 100081, China

23 [8] present address: Graduate School of Bioagricultural Sciences, Nagoya University,
24 Nagoya 464-8601, Japan
25 [9] present address: Multidisciplinary Science Cluster, Kochi University, Nankoku, Kochi,
26 783-8502, Japan
27 [10] present address: Biology Department, University of Massachusetts, Amherst, MA
28 01003 USA
29 * These authors contributed equally to this paper.
30 ** Author for correspondence
31

**Abstract**

Diverse wild and weedy crop relatives hold genetic variants underlying key evolutionary innovations of crops under domestication. Here, we provide genome resources and probe the genetic basis of domestication traits in green millet (*Setaria viridis*), a close wild relative of foxtail millet (*S. italica*). Specifically, we develop and exploit a platinum-quality genome assembly and *de novo* assemblies for 598 wild accessions to identify loci underlying a) response to climate, b) a key 'loss of shattering' trait that permits mechanical harvest, and c) leaf angle, a major predictor of yield in many grass crops. With CRISPR-Cas9 genome editing, we validated *Less Shattering1* (*SvLES1*) as a novel gene for seed shattering, which is rendered non-functional via a retrotransposon insertion in *SiLes1*, the domesticated loss-of-shattering allele of *S. italica*. Together these results and resources project *S. viridis* as a key model species for complex trait dissection and biotechnological improvement of panicoid crops.

46 **Introduction**

47 Warm season $C_4$ grasses (subfamily Panicoideae) such as maize, sorghum and
48 most species of millet are mainstays of industrial and small-holder agriculture, and
49 include most major biofuel feedstocks. Crucially, $C_4$ photosynthesis is most productive
50 under the hot and dry conditions that are predicted to become more prevalent over the
51 coming decades[1-3]. While contemporary breeding of Panicoideae crops targets a trade-
52 off between stress tolerance and yield, de novo domestication of wild Panicoideae
53 species may provide an alternative path to develop novel bioproducts, fuels and food
54 sources. However, the plants in the Panicoideae are known for long lifespans and large
55 or complex genomes, creating the need for a practical experimental model that can be
56 used for rapid discovery of gene structure and function and biotechnological
57 improvement of related crops.

58 *Setaria viridis* (green foxtail) has emerged as such a model[4-6]. Plants are small
59 (Figure 1a), diploid, have a short life cycle (seed to seed in 8-10 weeks), a small
60 genome (ca. 500 Mb), and are self-compatible, with a single inflorescence that often
61 produces hundreds of seeds. Transformation is efficient, and amenable to CRISPR-
62 Cas9 mediated mutagenesis. These features have enabled use of *S. viridis* for studies
63 of photosynthetic mechanisms[7-11], drought tolerance[12], cell wall composition[13-15], floral
64 and inflorescence development[16,17], leaf anatomy[18], secondary metabolism[19], plant
65 microbiomes[20,21], aluminum tolerance[22], defense responses[23], and even inspiration for
66 engineering applications[24] (Figure S1).

67 As in most wild species, seeds of *S. viridis* fall off the plant at maturity, a process
68 known as shattering[25]. While essential for dispersal in natural ecosystems, shattering is

69 undesirable in cultivation and humans have selected for non-shattering mutants since
70 the dawn of agriculture[26-28]. Such domesticates include *Setaria italica* (foxtail millet), the
71 domesticated form of *S. viridis*, which is grown as a crop in Asia[29-31]. Improvement of
72 some current crops (e.g. African fonio and North American wildrice) is hindered
73 because shattering causes high losses at harvest[32-34]. Thus identification of genes

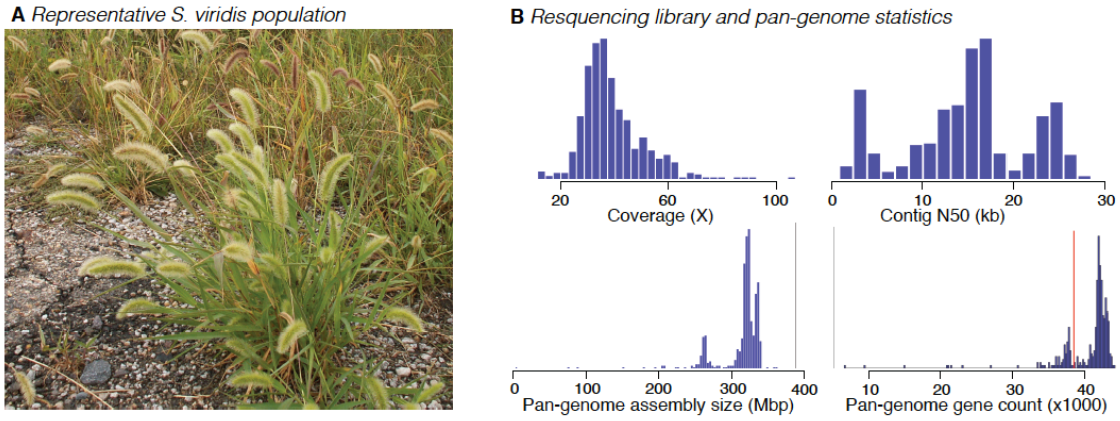


**Fig. 1. a** *Setaria viridis*, in its common highly disturbed habitat next to a road. **b** Average library coverage, contig N50 (Kb), pan-genome assembly size, and number of genes per library; red vertical line in lower right panel represents the number of genes necessary for a library to be included for PAV analysis (n=39,000).

74

75 critical for shattering has direct agronomic benefit.

76 Human selection on wild grasses could only have been effective if there is
77 standing variation in genetic loci that affect shattering. However, to our knowledge no
78 previous study has succeeded in cloning such loci via association studies of natural
79 diversity. Most previous efforts have instead relied on crosses between domesticated
80 plants and their wild progenitors, and genes and QTL identified in such studies are, for
81 the most part, not conserved among species[25,35,36]. We infer that many shattering-
82 related loci remain to be identified.

83 In the work reported here, we surveyed natural populations of *S. viridis* and found
84 allelic variation at a novel locus associated with seed shattering. We deployed a large
85 sequence-based resource for *S. viridis*, analyzed its population structure using single-
86 nucleotide polymorphisms (SNPs) and presence-absence variation (PAV) of individual
87 genes, and tested for signatures of selection. Genome-wide association studies
88 (GWAS) identified QTL for response to the abiotic environment and also a shattering-
89 related locus, *Less shattering1* (*Les1*). Function of *Les1* was validated with genome
90 editing. The orthologous gene in *S. italica* is disrupted by a transposon, indicating that
91 the locus also contributed to domestication. In a parallel study, we identified a locus
92 controlling leaf angle, a trait with clear agronomic implications. Data presented here
93 show that genomics and biotechnological resources in *S. viridis* can be used to
94 accelerate our mechanistic understanding of genetic processes and thereby contribute
95 to enhanced and stabilized yield.
96
97 **A complete genome and genomic model for the Panicoideae**
98 We have developed significant new resources for the *Setaria* community. A new
99 assembly was generated for the *S. viridis* reference line 'A10.1', using a combination of
100 long-read Pacbio and Illumina sequencing technologies. The final version 2.0 release is
101 a complete telomere-to-telomere chromosomal assembly, containing 395.1 Mb of
102 sequence in 75 contigs with a contig N50 of 11.2 Mb and a total of 99.95% of
103 assembled bases in nine chromosomes. This is a major improvement over previous *S.*
104 *viridis* genome releases, which had a contig N50 of 1.6 MB, and ca. 94% of reads in
105 contigs. The associated gene annotation is equally complete (BUSCO score [37] on

106 Embryophyta for the gene set v2.1 is 99%) describing 38,334 gene models and 14,125
107 alternative transcripts.
108 To complement the genome assembly and probe the genetic architecture of
109 complex traits we conducted deep resequencing (mean of 56M high quality paired end
110 reads, 42.6X coverage) of 598 *S. viridis* diversity samples using Illumina 2x150 paired
111 end (PE) libraries (Figure 1b; metadata and sequence accession numbers in Table S1).
112 Each library was subsequently assembled into a pan-genome database. While less
113 contiguous than the long-read based A10.1 genome (mean n. contigs: 75,001; Contig
114 N50: 16.2 Kb), total assembled bases were very similar (mean assembled bases =
115 322.5 M) (Figure 1b).
116
117 **Multiple introductions from Eurasia underlie distinct North American gene pools**
118 The history of *S. viridis* in North America is unknown, although previous phylogenetic
119 studies place it within a clade of Asian genotypes [38,39]; indicating that Eurasia is the
120 native range while North America represents a recent and likely human-associated
121 range expansion. To understand the relationship of the North American samples to
122 samples from the Old World, we called 8.58M single nucleotide polymorphisms (SNPs)
123 among our 598 Illumina libraries (Table S1). We then extracted polymorphisms
124 comparable to the genotype-by-sequencing (GBS) data from previously-published
125 Illumina sequence data for 89 non-US samples collected in China, Canada, Europe and
126 Middle East [40]. We then tested for population structure using fastStructure [41] and
127 Admixture [42]. Overall, we find four distinct subpopulations, all of which are found both in
128 North American and Eurasia (Figure 2a, b). This pattern is expected if *S. viridis*

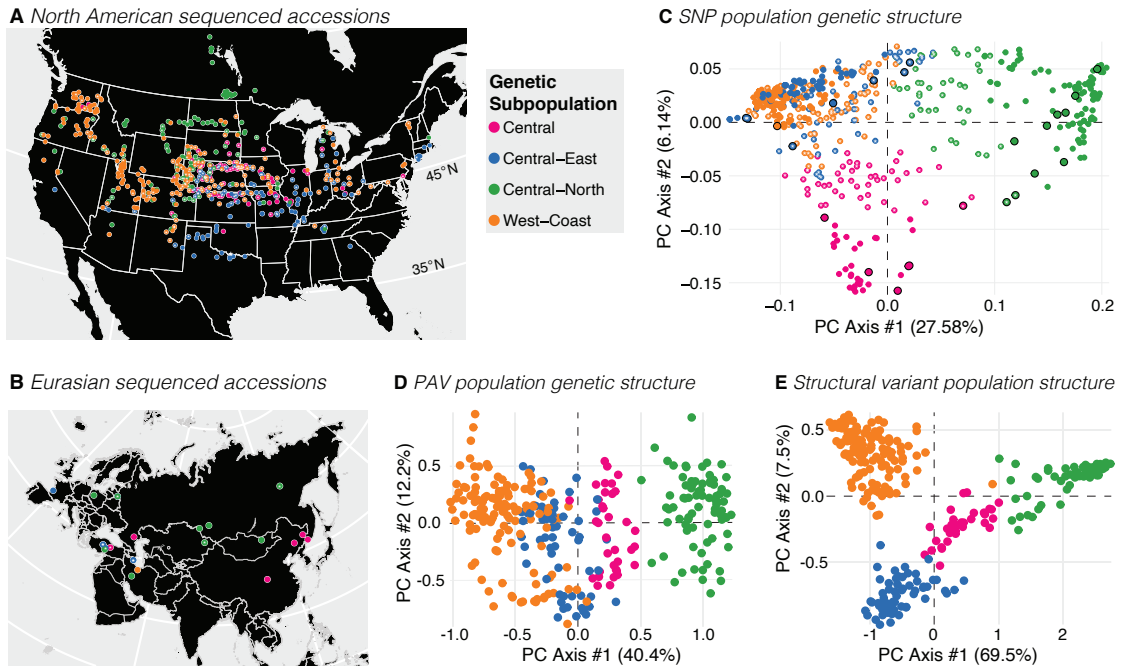


**Fig. 2.** PAV and SNP diversity of subpopulations. **a** Geographic distribution and population assignment of North American accessions based on SNP data. **b** Geographic distribution and population assignment of Eurasian accessions based on SNP data. **c** PCA of SNP data, showing placement of North American samples among Eurasian ones. **d** PCA of PAV variants, excluding admixed individuals. **e** PCA of structural variants, excluding admixed individuals. Both SNP and PAV data clearly separate the Central-North population (green) from the others, and the structural variants distinguish all populations. *, accession is admixed; black rim on circle, accession is in its native range.

diversified throughout Eurasia, was introduced to North America from several different sources, and then dispersed widely.

To define the evolutionary and biogeographical history of North American *S. viridis*, we conducted an identical population structure analysis with all SNPs in our resequencing panel. Of the 8.58 million SNPs (one SNP for every 21.6 bp), 430K mapped to exons (primary transcripts), 182K SNP were missense, 5K were nonsense, and 243K were silent. As with the GBS data, this analysis identified four main sub-populations (Central; Central-East; Central-North; West-coast; Figure S2). Not all individuals clustered uniquely into a single subpopulation; 382 genotypes were ‘pure’

139 and assigned to a single subpopulation while 216 individuals were 'admixed' (Q < 0.7).
140 These subpopulations trace their origins to distinct Eurasian gene pools: the 'Westcoast'
141 subpopulation was closely related to samples from a genetic subpopulation that
142 spanned the northern Middle East region; the closest relatives of the USA 'Central-
143 North' subpopulation were found from northern Europe through Siberia; the Eurasian
144 members 'Central-East' subpopulation were restricted to northern Iran and Afghanistan;
145 and samples from China exclusively group with the 'Central' USA subpopulation (Figure
146 2b, c). The Central USA population, whose Eurasian relatives inhabit a range from
147 China to Turkey, had the highest SNP diversity, highest number of private alleles, and
148 lowest mean linkage disequilibrium (LD) of all the populations (Table S2). Such elevated
149 diversity could be driven by larger or multiple founding populations.
150

151 **Pan-Genome gene presence-absence variation mirrors SNP diversity**

152 While SNPs serve as excellent proxies of total genetic diversity, previous work
153 has demonstrated that larger-scale variation such as gene presence-absence and
154 structural variants may underlie adaptation in nature and crop improvement[43-46]. To
155 capture the set of all genes in all accessions of *S. viridis* (i.e., the pan-genome), we
156 needed to identify genes that were missing or not annotated in the v2.1 gene set
157 reference. Accordingly, we identified proteins in *Setaria italica* (v2.2), *Zea mays*
158 (v.PH207) and *Sorghum bicolor* (v3.1) that were not shared with (i.e., not orthologous
159 to) those in *S. viridis* (v2.1) and determined which were present in at least one member
160 of the non-admixed diversity panel (382 accessions). This set of proteins was then
161 added to the set from *S. viridis* (v2.1) to identify a pan-genome of 51,323 genes. Within

162 this pan-genome, a core set of 39,950 genes occurred in 98% of all individuals. Of
163 these core genes 32,732 were annotated in *S. viridis* (v2.1), with 3224, 3412, and 582
164 more identified based on similarity to *S. italica*, *Z. mays* and *S. bicolor* gene models,
165 respectively. Discriminant function analysis of principal components (DAPC)[47,48], a
166 multivariate method for identifying clusters of genes, identified an additional 5385 genes
167 in 56% of all individuals (the "shell" set), and found the remaining 5987 in 12% of all
168 individuals (the "cloud").

169 Consistent with other studies of pan-genome population genetics[49], the SNP- and
170 PAV-based estimates of subpopulation structure are similar. Analysis of the "shell" gene
171 PAV data revealed four subpopulations (n = 130, 78, 59, 35, respectively; Fig. 2d). Of
172 the 203 non-admixed genotypes (that also had sufficient PAV data), 190 (94%)
173 assigned to the same genetic subpopulation as in the SNP analysis. The Central-North
174 population is clearly distinct in both PAV and SNP data (Fig. 2c), and when all structural
175 variants are considered, the four populations are distinct (Fig. 2e). 4,062 genes are
176 significantly over- or under-represented among subpopulations ($P < 0.05$; $X^2$- test, with
177 Benjamini-Hochberg correction), with 45 private alleles (MAF > 0.1) specific to particular
178 subpopulations (Table S3). KEGG and GO enrichment analyses for over-represented
179 genes in each population found pathways relating to biosynthesis of secondary
180 compounds, and genes involved in defense response to pathogens or herbivores Figure
181 S3.

182 Our PAV data connect published QTL studies with population-level processes.
183 For example, a study of drought response in *S. viridis* found a strong-effect QTL
184 significant for plant size, water loss, and WUE across all tested environments [50].

185 Investigation within the pan-genome found an *S-phase kinase associated protein1*
186 (*Skp1)* homolog (Sevir.2G407800) within 50Kb of the associated SNP that was common
187 in the Central-North population (present in 65% of individuals), while significantly under-
188 represented in the Central-East (present in 5% of individuals) ($p < 4.3 \times 10^{-15}$). SKP1
189 proteins are part of the E3 ubiquitin ligase complex that leads to protein degradation[51];
190 while the physiological role of this particular SKP1 homolog is unknown, the fact that it
191 falls within a known QTL interval and is differentially represented in two populations
192 suggests it may be a candidate for future investigation.
193
194 **Selection and correlation with climate in the new range of *S. viridis***
195
196 Combined, the PAV and SNP data clearly demonstrate massive genetic diversity
197 and distinct gene pools to target molecular dissection of agriculturally important traits,
198 including response to the environment. While we have shown that genetic variation in
199 North American *S. viridis* reflects multiple introductions, we also observe pervasive
200 genetic and biogeographic admixture. These factors, combined with its rapid cycling
201 and weedy life history, indicate that adaptation to climate may underscore a
202 biogeographic range expansion across much of the continent. To test this hypothesis,
203 we characterized the environment for each accession using principal components
204 analysis (PCA) of the Worldclim[52] environmental variables. To overcome collinearity
205 among the climate variables (Figure S4), we transformed the 19 variables into the first
206 three principal components (36.13%, 30.07% and 16.36% variance explained; factor
207 loadings in Table S4), which served as response variables for three GWAS analyses.
208 To control for population structure, we also supplied a set of three SNP-derived kinship
209 PC axes which explain 15.34% of the genetic relatedness in our panel.

210 While the first bioclimatic PC axis was not significantly associated with any SNP
211 markers, PC2 had one association (Chr01: 37,770,697) (Figure S5) and PC3 identified
212 several peaks with a total of 140 significant markers (Bonferroni corrected p-value,
213 5.82e-09). PC3 is loaded by climatic variables relating to extremes of precipitation and
214 temperature. Of the 140 PC3 hits, 66 fall within 16 genes (Table S5). Genes within 100
215 Kbp of the significant markers were associated with organellar genome maintenance
216 (GO:0033259, GO:0000002, GO:0006850), protein breakdown (GO:0045732),
217 gibberellic acid homeostasis (GO:0010336), and fucose metabolism (GO:0006004,
218 GO:0042353) (Table S6).
219 Despite the relatively small number of clear associations with parameters of the
220 abiotic environment, both Tajima's D and iHS found multiple genes under selection in
221 the four populations (Figure S6; Table S7). The two tests have different underlying
222 assumptions and methods; genes that appear as outliers in both tests and annotations
223 that arise repeatedly are excellent candidates for further investigation. For example, in
224 most subpopulations we find selected genes consistently enriched in flavonoid (and
225 other derivatives of phenylalanine) metabolism GO terms and KEGG pathways,
226 processes that are often underlie responses to herbivores and pathogens and could be
227 involved in local adaptation. However, selection on other processes and pathways
228 appears to be specific to only one subpopulation. For example, genes involved in pH
229 reduction in the Central-North population are identified by both tests, although
230 interpretation of this result would require investigation of individual sets of genes and
231 their tissue localization. Together, the bioclim GWAS and tests for selection show that
232 *S. viridis* can provide testable hypotheses of gene function and phenotypic output.

233
234 **A novel gene, *SvLes1*, controls seed shattering in *S. viridis***

235 We deployed the new high quality genome, pan-genome and population genetic
236 analyses to link genotypic diversity to the agronomically important phenotype of reduced
237 shattering. We tested a subset of lines for seed shattering using a simple shattering
238 index, in which mature panicles were scored for shattering on a scale of 1 (low) to 7
239 (high; Table S8). GWAS identified a single strong QTL (peak $-\log_{10} P > 30$) for seed
240 shattering on chromosome 5 (Figure 3a) a region of approximately 2Mb above the
241 experiment-wise p=0.01 Bonferroni correction threshold. In this region, 119 mutations,
242 primarily missense, alter protein sequences relative to the reference; we used
243 PROVEAN[53] to predict deleterious mutations that are more likely to alter the biological
244 function of protein products. Combining this prediction and the association score of
245 SNPs (Figure 3b), we prioritized a single G-T polymorphism (Chr_05:6849363) in a
246 gene encoding a MYB transcription factor, *SvLes1* (Sevir.5G085400, similar to
247 Sobic.003B087600 from *Sorghum bicolor* and ZM00001d040019_T001 from *Zea*
248 *mays*), with two MYB DNA-binding domains. The mutation leads to a R84S substitution
249 in the second MYB domain of *SvLes1* (Figure 3c). We name these two alleles *SvLes1-*
250 *1* and *SvLes1-2*, associated with high seed shattering and reduced shattering,
251 respectively. The *SvLes1-2* allele appears in 24% of the 215 accessions of the GWAS
252 panel, and clearly associates with reduced shattering scores (p=6.53E1-33, 2-tailed
253 test; Table S8). The reference line A10.1 is among these reduced-shattering lines.

254 To validate *SvLes1* as the causal gene, we used CRISPR-Cas9 to create
255 additional alleles. We disrupted the wild type, high-shattering allele *SvLes1-1* in the
256 accession ME034v (corresponding to accession TB0147) to create several novel, non-

257 functional alleles. Sequence analysis of *SvLes1-CRISPR1* revealed an adenine

258 insertion at position 149 of the transcript (Figure 3d), leading to a frameshift mutation

259 predicted to completely abolish gene function thereby creating non-shattering plants.

260 After segregating out the transgenes encoding Cas9 and guide RNAs, homozygotes of

261 *SvLes1-CRISPR1* were phenotypically examined in the T3 generation.

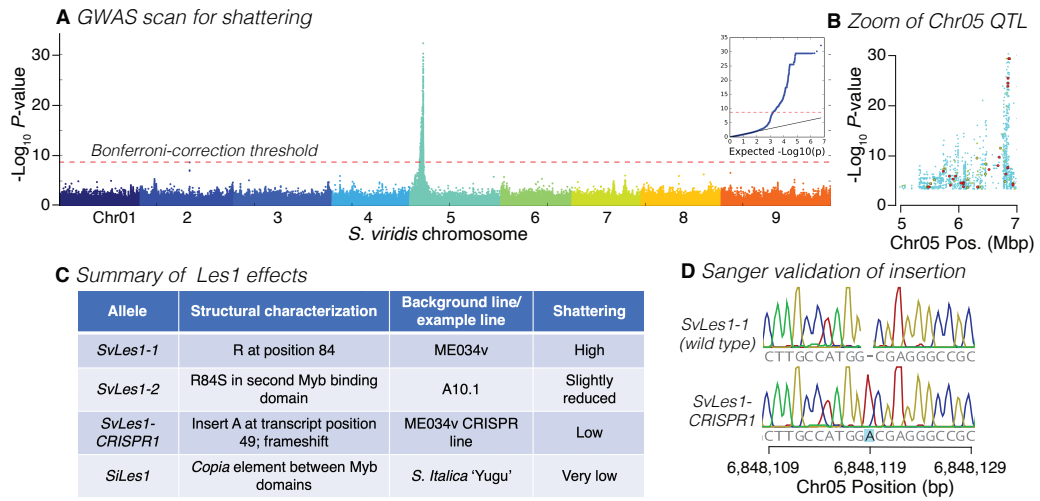


| Allele | Structural characterization | Background line/ example line | Shattering |
|---|---|---|---|
| *SvLes1-1* | R at position 84 | ME034v | High |
| *SvLes1-2* | R84S in second Myb binding domain | A10.1 | Slightly reduced |
| *SvLes1-CRISPR1* | Insert A at transcript position 49; frameshift | ME034v CRISPR line | Low |
| *SiLes1* | *Copia* element between Myb domains | *S. Italica* 'Yugu' | Very low |

**Fig. 3.** GWAS and cloning of *Les1*. **a** Manhattan plot of GWAS result, red line showing p=0.01 after Bonferroni correction. **b** Zoom in to peak on Chromosome 5; larger dots represent missense SNPs identified by snpEff. Different colors of missense SNPs indicate Provean score range (blue for >-2.5, green for <-2.5 and >-4.1, red for <-4.1; -2.5 and -4.1 represent 80% and 90% specificity). Lower scores indicate higher likelihood of deleterious effects of the mutation. **c** Table of *Les1* alleles in *S. viridis* (*Sv*) and *S. italica* (*Si*), with structural characteristics, background line, and shattering phenotype. **d** Sanger sequence validating the position of the adenine insertion (frameshift) in *SvLes1-CRISPR-1*.

262

263 To quantify seed shattering, we measured tensile strength of the abscission zone

264 (AZ)[54,55]. We compared *SvLes1-CRISPR1* and *SvLes1-1*(both in an ME034v

265 background) with *SvLes1-2* (in the A10.1, reduced shattering, background). *SvLes1-1*

266 had the lowest tensile strength (high shattering), *SvLes1-2* tensile strength was slightly

267 higher (less shattering), and *SvLes1-CRISPR1* had high tensile strength (reduced seed

shattering) (Figure 4a,b). These results were confirmed with wind tunnel experiments measuring the number of seeds released from the inflorescence and the distance they traveled (Figure 4c). Few *SvLes1-CRISPR1* seeds were released from the plant, whereas dozens of seeds were released from the *SvLes1-1* plants at six weeks after heading. Seeds of the *SvLes1-CRISPR1* allele weighed significantly less than in

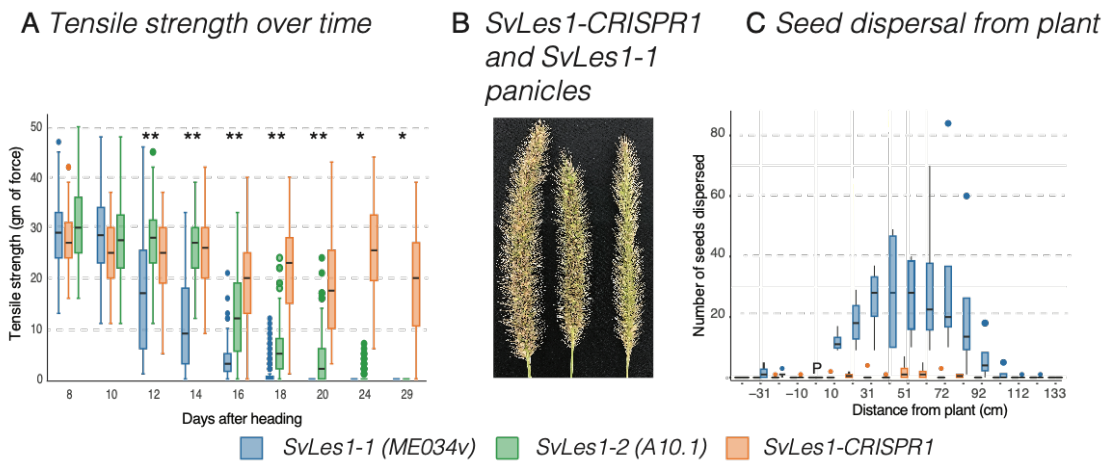


**Fig. 4.** Phenotypic characterization of *SvLes1-CRISPR1* mutants and naturally occurring alleles. **a** Force required to break the AZ (tensile strength in gm of force) in *SvLes1-1*, *SvLes1-2*, and *SvLes1-CRISPR1* lines, measured every two days starting at 8 days after heading. **b** Image of *S. viridis* high shattering (*SvLes1-1* in ME034), left two panicles) and *SvLes1-CRISPR1* mutant panicles seven weeks after heading. Both mutants have retained their seed, unlike ME034 which has shed most of its seed at this time point. **c** Seed dispersal distances in a wind tunnel, measured from four independent high shattering plants (*SvLes1-1* in ME034) and eight *SvLes1-CRISPR1* plants at week 6. Wind speed was 5 mph coming from the left of the diagram. The plant, indicated by P, was placed in middle of the tunnel; some seed fell on the windward side (negative distance values) due to oscillation of the plant. Although mean dispersal distance was approximately the same for both alleles, the *SvLes1-CRISPR1* plants released significantly fewer seeds at each distance that the *SvLes1-1* plants.

*SvLes1-1*, but germination percentage was unaffected (Figure S7). T3 offspring of T2 heterozygous plants segregated 3:1 shattering to non-shattering as expected for an

276 induced mutation in a single gene, implying that the lines are isogenic except for the
277 mutant allele.

278 *SvLes1* is a transcription factor that has not been implicated in shattering in any
279 other species. Despite studies identifying shattering related genes in rice (e.g. *Sh4*[55],
280 *qSh1*[56], *Shat1*[57]) and sorghum (e.g. *Sh1*[58]), the cellular mechanism of shattering is not
281 known in any cereal, and recent data suggest that each species may be unique[36].
282 Unlike other grasses, the AZ in *Setaria viridis* is not histologically distinct and is only
283 subtly different from that in *S. italica*[25,54]. Cells and cell walls in the AZ are not clearly
284 different from their neighboring cells (demonstrated by multiple different cell wall stains
285 plus TEM[36]). Given this histology, we expected that the AZ of non-shattering mutants
286 would look like that of wild type plants, and indeed the anatomy and histology of
287 *SvLes1-CRISPR1* and *SvLes1-1*spikelets are indistinguishable (Figure S8).
288

289 **Recent transposable element insertion in *S. italica Les1* contributed to**
290 **domestication of foxtail millet**

291 Because *Setaria italica* (foxtail millet) is a domesticated (non-shattering)
292 derivative of *S. viridis*[29-31], we hypothesized that selection of non-shattering lines could
293 have identified rare alleles of *S. viridis* or *S. italica* early in the domestication process.
294 We discovered a ~6.5kb *copia* transposable element (*copia38*) inserted between the
295 two Myb domains of *SiLes1* in the *S. italica* line Yugu1. We call this the *SiLes1-TE*
296 (transposable element) allele. The disruption of the Myb domain strongly suggests
297 *SiLes1-TE* is a loss of function allele similar to *SvLes1-CRISPR1* and should also
298 produce a low shattering phenotype, thus potentially contributing to the domestication of

299 foxtail millet. The *copia38* transposable element was aligned to each of the 598 *S.*
300 *viridis* re-sequenced lines to investigate whether any had the TE insertion in *SvLes1*.
301 Only two samples aligned to the *copia38* TE within the CDS sequence of *SvLes1*, but
302 the nucleotide identity and coverage of the alignments were poor (32% and 6%
303 respectively). In contrast, *Copia38* is nearly fixed among the foxtail millet lines
304 examined (78 out of 79).

305 Genome-wide, *S. italica* has about 22% of the SNP variation of *S. viridis* (based
306 on sequences generated in [59]), as expected given its domestication history. In the
307 *SiLes1* region, however, this number is significantly reduced to 4.1-8.2% of the diversity
308 in *S. viridis* depending on the size of the region compared (10-100 Kbp, Table S9)
309 ($p=0.0066$ based on 100,000 coalescent simulations of the ratio of $\pi$ *italica*/$\pi$ *viridis*).
310 These data hint that the low-shattering QTL might co-localize with a selective sweep.
311 Diversity is relatively high within the *S. italica* gene itself, which may mean that selection
312 is on a regulatory region or additional locus under the QTL or that the transposon
313 insertion has rendered *SiLes1* a pseudogene. Estimates of linkage disequilibrium (LD)
314 support this interpretation (Table S10). In *S. viridis* estimates of LD do not vary much
315 across intervals from 10 to 100 Kbp surrounding *SvLes1*. In *S. italica* on the other hand,
316 LD is nearly complete for the 20 kb region surrounding *SiLes1*. When that region is
317 expanded to 40 Kbp LD drops to levels approximating that in *S. viridis*. Taken together,
318 these data indicate either a selective sweep or purifying selection on a genomic region
319 that includes *SiLes1* and *copia38* in LD.

320 *SiLes1* has not been identified in other studies of *S. italica* and thus its potential
321 role in domestication is newly described here. Two strong QTL for shattering were

322 identified in recombinant inbred lines derived from an *S. italica* x *S. viridis* cross
323 (accessions B100 and A10.1, respectively)[60], but neither QTL encompasses *SiLes1*.
324 Analysis of 916 diverse accessions of *S. italica* identified 36 selective sweeps, but the
325 *SiLes1* region does not colocalize with any of them[59]. In addition, a previous study[54]
326 found that tensile strength in two elite *S. italica* lines, Yugu1 and B100, is higher than
327 that of the *SvLes1-CRISPR1* homozygotes reported here. Thus all previous data
328 indicate that *SiLes1-TE* is but one of several loci contributing to the lack of shattering in
329 foxtail millet.

330 *Copia38* is a long terminal repeat (LTR) retroelement with two 451 bp LTR
331 sequences. The LTRs for *Copia38* are identical across the entire pan-genome,
332 suggesting that the insertion is recent, because mutations start to accumulate in the
333 once-identical LTRs immediately after insertion of a TE. Phylogenetic analysis showed
334 *Copia38* tightly clusters with a few homologous copies on a long branch, indicating a
335 shared burst event for copies in this cluster (Figure S9). Pairwise distance among the
336 copies suggests this burst was recent, on average about 45k (range 23k – 81k) years
337 ago, assuming a neutral mutation rate of $6.5\times10^{-9}$/bp/year[61]. The copies from this burst
338 only occur in Yugu1 but not in A10.1, suggesting a recent expansion just prior to
339 domestication of *S. italica* that began approximately 8000 years ago[29-31].

340 Combining the results and evidence above, a plausible scenario is that the
341 *SiLes1-TE* allele was a low frequency allele that was selected during domestication due
342 to its favored low shattering phenotype, and spread quickly through the early foxtail
343 millet land races. Later, the low shattering phenotype was further strengthened by
344 additional loci with stronger effects (i.e. *SvSh1*[59,60]) during recent crop improvement.

345 Genome editing technology today allows us to recreate a low-shattering phenotype from
346 ancestral *S. viridis* alleles, mimicking the initial phase of foxtail millet domestication
347 through a different novel allele *SvLes1-CRISPR1.*
348

349 **Parallel genetic control of leaf angle in *S. viridis* and maize by *liguleless2***
350 **orthologs**

351 The diversity panel is also a powerful tool for uncovering the basis of rare traits,
352 including those of agronomic value. We discovered a single accession in the panel
353 (TB0159) with reduced auricle development and markedly upright leaves (small leaf
354 angle) (Figure 5a,b), a trait of considerable interest in the major crops maize and rice,
355 where it has led to increased planting densities and higher yields[62-64]. As GWAS is not
356 suitable for mapping traits with low frequency and strong effects, bulked segregant
357 analysis (BSA)[17,40] was used to identify the associated genomic region. BSA is a
358 process in which plants with and without a particular phenotype are pooled (bulked) and
359 then each pool is sequenced. Regions or loci that differ between the two pools are then
360 inferred to contain the mutations underlying the phenotype. TB0159 was crossed to
361 A10.1, and the F1 plants showed wild type leaf angle, showing that small leaf angle is
362 recessive. The wild type and small leaf angle trait in the $F_2$ population segregated at
363 264:153 which differs significantly from a 3:1 ratio (p=0.000238). This could be
364 explained by partial dominance at a single locus, or by several loci controlling the
365 phenotype. We proceeded assuming a single partially dominant causal gene for small
366 leaf angle.
367

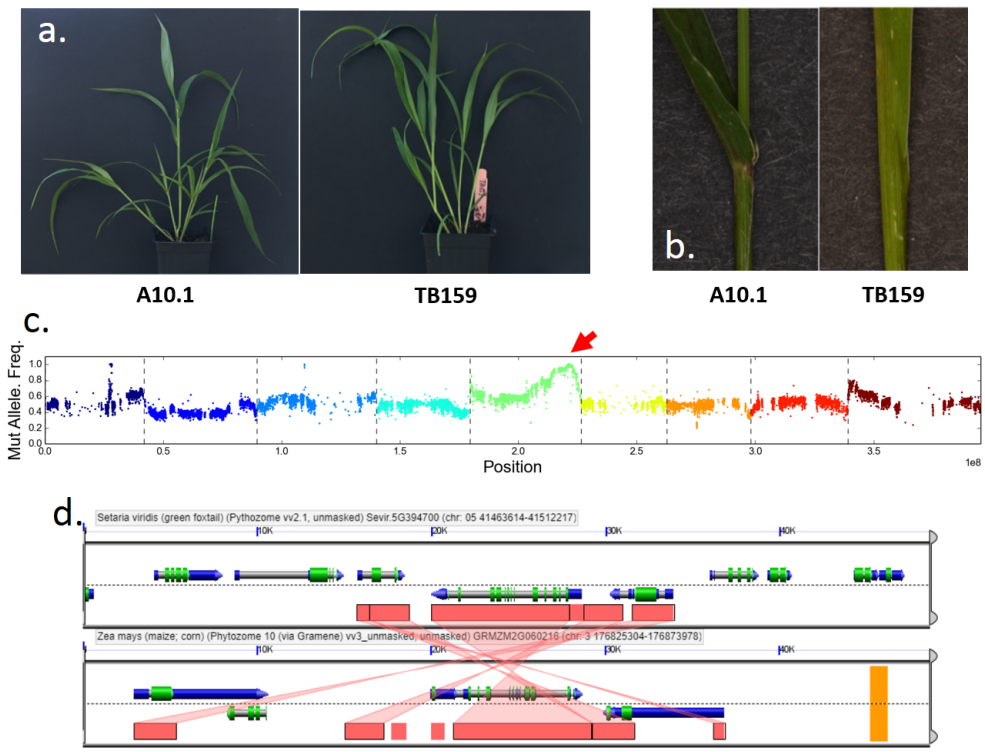


**Fig. 5.** Phenotype and mapping of small leaf angle. **a, b** Small leaf angle phenotype in TB159. **c** BSA mapping result, red arrow indicating QTL. **d** Synteny analysis around *SvLg2* and maize *lg2* locus.

With BSA, we coarsely mapped the reduced leaf angle phenotype to a homozygous region of ~800 kb on chromosome 5 (Figure 5c) that contained 104 disruptive SNPs and 687 indels (393 single bp). This region includes *SvLiguless2* (*SvLg2*) (Sevir.5G394700), the syntenic ortholog of *liguless2* in maize (Figure 5d), which is a transcriptional regulator that controls auricle development and leaf angle[65]. Because the small leaf angle phenotype is partially dominant and unique to TB0159 in the panel, the causal allele should be homozygous and occur only in that accession. We identified a homozygous G insertion (Chr_5:41489494) in the coding region of *SvLg2* of that is predicted to cause a frameshift. Accordingly, we hypothesize that this indel mutation might be the causal mutation for the small leaf angle in TB0159. As the ligule is a trait

379 unique to grasses and has been a target for breeding programs, *S. viridis* can now be
380 used as a model system to rapidly dissect the molecular genetic network of Lg2, which
381 remains poorly resolved in maize and rice, to identify additional candidates for breeding
382 or engineering of this important architectural trait.

383 In summary, data presented here demonstrate the power of the *S. viridis* genome
384 and associated diversity lines for gene discovery. Together these tools permit discovery
385 of novel environmental associations and genes such as *SvLes1*, and additional insight
386 into genes such as *SvLg2* that have been identified from related systems. We show that
387 *S. viridis* resources can uncover the genetic basis of a trait when the genes are
388 unknown and likely differ from those in other related species. We also show that *S.*
389 *viridis* can be a model for investigating genes in which an orthologue is known in a crop.
390 Specifically, we have used the *S. viridis* genome and diversity panel to study the genetic
391 basis of seed shattering and leaf angle (*SvLes1* and *SvLg2*, respectively), traits that
392 influence crop yield by affecting harvestability, productivity and density of planting.
393

394 **Methods**

395

396 **Plant materials**

397 The reference line A10.1 is a descendant of the line used by Wang et al.[66] in early
398 RFLP maps. The original line was found to be heterozygous and thus A10.1 was
399 propagated via single-seed descent by Andrew Doust (Oklahoma State University,
400 Stillwater, OK, pers. comm.). It is thought to have originated in Canada. The other
401 reference, ME034 (also known as ME034v), was collected by Matt Estep (Appalachian

402 State University, Boone, NC) in southern Canada as part of a diversity panel[39] included
403 among the diversity lines sequenced here. Transformation is more efficient for ME034
404 than for A10.1 (Joyce van Eck, Boyce Thompson Institute, Ithaca, NY, pers. comm.)
405 and thus the former is being used widely for functional genetic studies.
406 The 598 individuals of the diversity panel were collected over a period of several
407 years. About 200 lines have been described in previous studies[39,67] whereas others
408 were new collections added for this project. Individuals were propagated by single seed
409 descent, although the number of generations varies by accession. *Setaria viridis* is
410 inbreeding by nature (ca. 1%[67]), so we assume that initial heterozygosity was generally
411 low and then further reduced in propagation.
412
413 **Library creation and sequencing**
414 To prepare DNA for sequencing of the reference line, 100 ng of DNA was
415 sheared to 500 bp using the Covaris LE220 (Covaris) and size selected using SPRI
416 beads (Beckman Coulter). The fragments were treated with end-repair, A-tailing, and
417 ligation of Illumina compatible adapters (IDT, Inc) using the KAPA-Illumina library
418 creation kit (KAPA biosystems). The prepared library was then quantified using KAPA
419 Biosystem's next-generation sequencing library qPCR kit and run on a Roche
420 LightCycler 480 real-time PCR instrument. The quantified library was then multiplexed
421 with other libraries, and the pool of libraries was prepared for sequencing on the
422 Illumina HiSeq sequencing platform using a TruSeq paired-end cluster kit, v3, and
423 Illumina's cBot instrument to generate a clustered flowcell for sequencing. Sequencing

424 of the flowcell was performed on the Illumina HiSeq2000 sequencer using a TruSeq
425 SBS sequencing kit, v3, following a 2x150 indexed run recipe.
426 Plate-based DNA library preparation for Illumina sequencing was performed on
427 the PerkinElmer Sciclone NGS robotic liquid handling system using Kapa Biosystems
428 library preparation kit. 200 ng of sample DNA was sheared to 600 bp using a Covaris
429 LE220 focused-ultrasonicator. Sheared DNA fragments were size selected by double-
430 SPRI and then the selected fragments were end-repaired, A-tailed, and ligated with
431 Illumina compatible sequencing adaptors from IDT containing a unique molecular index
432 barcode for each sample library.
433 The prepared library was quantified using Kapa Biosystem's next-generation
434 sequencing library qPCR kit and run on a Roche LightCycler 480 real-time PCR
435 instrument. The quantified library was then multiplexed with other libraries, and the pool
436 of libraries was then prepared for sequencing on the Illumina HiSeq sequencing
437 platform using a TruSeq paired-end cluster kit, v3 or v4, and Illumina's cBot instrument
438 to generate a clustered flowcell for sequencing. Sequencing of the flowcell was
439 performed on the Illumina HiSeq2000 or HiSeq2500 sequencer using HiSeq TruSeq
440 SBS sequencing kits, v3 or v4, following a 2x150 indexed run recipe.
441
442 **Sequencing of the reference genome**
443 We sequenced *S. viridis* A10.1 using a whole genome shotgun sequencing strategy and
444 standard sequencing protocols. Sequencing reads were collected using Illumina HISeq
445 and PACBIO SEQUEL platforms at the Department of Energy (DOE) Joint Genome
446 Institute (JGI) in Walnut Creek, California and the HudsonAlpha Institute in Huntsville,

447 Alabama. One 800 bp insert 2x250 Illumina fragment library (240x) was sequenced,
448 giving 425,635,116 reads (Table S11). Illumina reads were screened for mitochondria,
449 chloroplast, and PhiX contamination. Reads composed of >95% simple sequence were
450 removed. Illumina reads <75bp after trimming for adapter and quality (q<20) were
451 removed. For the PACBIO sequencing, a total of 36 P5C2 chips (4 hour movie time)
452 and 41 P6C4 chips (10 hour movie time) were sequenced with a p-read yield of 59.09
453 Gb, with a total coverage of 118.18x (Tables S11, S12).
454
455 **Genome assembly and construction of pseudomolecule chromosomes**
456 An improved version 2.0 assembly was generated by assembling 4,768,857 PACBIO
457 reads (118.18x sequence coverage) with the MECAT assembler[68] and subsequently
458 polished using QUIVER[69]. The 425,635,116 Illumina sequence reads (240x sequence
459 coverage) were used for correcting homozygous snp/indel errors in the consensus.
460 This produced 110 scaffolds (110 contigs), with a contig N50 of 16.8 Mb, and a total
461 genome size of 397.9 Mb (Table S13). A set of 36,061 syntenic markers derived from
462 the version 2.2 *Setaria italica* release was aligned to the MECAT assembly. Misjoins
463 were characterized as a discontinuity in the *italica* linkage group. A total of 15 breaks
464 were identified and made. The *viridis* scaffolds were then oriented, ordered, and joined
465 together into 9 chromosomes using syntenic markers. A total of 61 joins were made
466 during this process. Each chromosome join is padded with 10,000 Ns. Significant
467 telomeric sequence was identified using the TTTAGGG repeat, and care was taken to
468 make sure that it was properly oriented in the production assembly.

469 Scaffolds that were not anchored in a chromosome were classified into bins
470 depending on sequence content. Contamination was identified using blastn against the
471 NCBI nucleotide collection (NR/NT) and blastx using a set of known microbial proteins.
472 Additional scaffolds were classified as repetitive (>95% masked with 24mers that occur
473 more than 4 times in the genome) (26 scaffolds, 1.2 Mb), alternative haplotypes
474 (unanchored sequence with >95% identity and >95% coverage within a chromosome)
475 (15 scaffolds, 1.0 Mb), chloroplast (3 scaffolds, 164.5 Kb), mitochondria (5 scaffolds,
476 344.9 Kb), and low quality (>50% unpolished bases post polishing, 1 scaffold, 19.3 Kb).
477 Resulting final statistics are shown in Table S14.
478 Finally, homozygous SNPs and INDELs were corrected in the release consensus
479 sequence using ~60x of Illumina reads (2x250, 800 bp insert) by aligning the reads
480 using bwa mem [70] and identifying homozygous SNPs and INDELs with the GATK's
481 UnifiedGenotyper tool [71]. A total of 96 homozygous SNPs and 4,606 homozygous
482 INDELs were corrected in the release. The final version 2.0 release contains 395.1 Mb
483 of sequence, consisting of 75 contigs with a contig N50 of 11.2 Mb and a total of
484 99.95% of assembled bases in chromosomes (Table S14).
485 Completeness of the v2.0 assembly is very high. To further assess completeness
486 of the euchromatic portion of the version 2.0 assembly, a set of 40,603 annotated genes
487 from the *S. italica* release was used for comparison. The aim of this analysis is to
488 obtain a measure of completeness of the assembly, rather than a comprehensive
489 examination of gene space. The transcripts were aligned to the assembly using BLAT [72]
490 and alignments ≥90% base pair identity and ≥85% coverage were retained. The
491 screened alignments indicate that 39,441 (97.14%) of the *italica* genes aligned to the

492 version 2.1 release. Of the unaligned 1,162 transcripts, 928 (2.28%) indicated a partial
493 alignment, and 234 (0.58%) were not found in the version 2.1 release.
494 To assess the accuracy of the assembly, a set of 335 contiguous Illumina clones
495 >20 Kb was selected. A range of variants was detected in the comparison of the clones
496 and the assembly. In 239 of the clones, the alignments were of high quality (< 0.01%
497 bp error) with an example being given in Figure S10a (all dot plots were generated
498 using Gepard [73]). The remaining 96 clones indicate a higher error rate due mainly to
499 their placement in more repetitive regions (Figure S10b). The major component of the
500 error in the 96 repetitive clones was copy number variation, which affected 50 of the
501 clones. These 50 clones accounted for >97% of all of the errors in the 335-clone set.
502 Excluding the clones with copy number variation, the overall bp error rate in the 285
503 clone set is 0.0098% (1,043 discrepant bp out of 10,601,785).
504
505 **Annotation**
506 Various Illumina RNA-seq reads were used to construct transcript assemblies using a
507 genome-guided assembler, PERTRAN[74]: 1B pairs of geneAtlas, 0.9B pairs of LDHH,
508 0.9B pairs of LLHC, and 176M other pairs. 109,119 transcript assemblies were
509 constructed using PASA[75] from RNA-seq transcript assemblies above.
510 Gene models of v1.1 on assembly v1.0 were lifted over to assembly v2.0 and
511 improved. The in-house gene model improvement (GMI) pipeline is as follows:
512 The genomic sequence of a locus is obtained, including introns if any and up to
513 1Kbp extensions on both ends unless they run into another gene. For intergenic space
514 less than 2Kbp, half of the intergenic distance is the extension for 2 adjacent loci. These

515 locus sequences are mapped to a new genome using BLAT. Duplicate mappings are
516 resolved using the gene model's neighbors in original genome space. When a locus
517 genomic sequence is mapped to the new genome uniquely and 100%, the gene model
518 is perfectly transferred to the new genome. For the remaining gene models, both their
519 transcript and CDS sequences are mapped with BLAT to the region in the new genome
520 located by locus genomic sequence mapping above. Gene models are made from CDS
521 alignments with quality of 95% identity, 90% coverage and valid splice sites if any, and
522 are transferred if the resulting peptide is 70% or more similar to the original gene model
523 peptide. UTRs are added if any using transcript alignments. Remaining gene models
524 are mapped to the new genome using GMAP. Gene models based on GMAP
525 alignments with quality of 95% identity, 70% coverage and valid splice sites if any are
526 transferred if and only if the resulting gene model peptide is 70% or more similar to the
527 original gene model peptides and in the new genome location not occupied by
528 transferred gene models in earlier steps.

529 Non-overlapping complete ORFs from each PASA transcript assembly (TA) were
530 predicted if the ORF had good homology support or was long enough (300bp if multi
531 exons or 500bp if single exon). Proteins from *Arabidopsis thaliana*, rice, sorghum,
532 *Brachypodium distachyon*, *Setaria italica*, grape, soybean and Swiss-Prot eukaryote
533 were used to score TA ORFs using BLASTP. The TA ORFs were then fed into the
534 PASA pipeline where EST assemblies were obtained for gene model improvement
535 including adding UTRs. PASA improved gene model transcripts were compared to v1.1
536 lifted over models on how well the transcript CDS was supported by ESTs and/or
537 homologous protein, and not overlapped with repeats generated with RepeatMasker[76]

538 for more than 20 percent. If PASA gene models of TA ORFs were better than lifted over
539 ones, the PASA gene models took over the lifted over ones. Otherwise, the lifted over
540 gene model stayed. The final gene model proteins were assigned PFAM, PANTHER
541 and gene models were further filtered for those with 30% or more of proteins assigned
542 to transposable element domains.

543 Locus model name was assigned by mapping forward v1.1 locus model if
544 possible using our locus name map pipeline; otherwise, a new name was given using
545 JGI locus naming convention that was used in v1.1 locus model naming. Our locus
546 name map pipeline is as following: a locus is said to be mapped and name mapped
547 forward if 1) the prior version and current version loci overlap uniquely and appear on
548 the same strand, and 2) at least one pair of translated transcripts from the old and new
549 loci are MBH's (mutual best hits) with at least 70% normalized identity in a BLASTP
550 alignment (normalized identity defined as the number of identical residues divided by
551 the longer sequence). For a given pair of prior version and current version transcripts at
552 mapped loci, transcript model names are mapped forward if either a) an MBH
553 relationship exists between the two proteins with at least 90% normalized identity or, b)
554 the proteins have at least 90% normalized identity and are not MBH, but the
555 corresponding transcripts sequences are (also with 90% normalized identity). This latter
556 rule is specifically to handle cases where the prior version and current version models
557 differ mainly by the addition of, or extension, of the UTR to a prior version model. These
558 rules allowed the model names of approximately 92% v1.1 gene models mapped
559 forward to v2.1.
560

561 **Sequencing and assembly of the diversity panel**

562 After excluding seven lines because of low sequence coverage, 598 diversity samples
563 (metadata, including Sequence Read Archive (SRA) numbers in Table S1) were used
564 for diversity analysis. The samples were sequenced using Illumina paired end
565 sequencing (2*151bp) at the Department of Energy Joint Genome Institute (JGI, Walnut
566 Creek, CA, USA) and the HudsonAlpha Institute for Biotechnology (Huntsville AL, USA)
567 using Hiseq 2500 and NovoSeq6000. Individual de novo assemblies for each line were
568 constructed using Meraculous (v2.2.5)[77] with a kmer size of 51, selected to maximize
569 the contig N50 in the resultant assemblies, and to ensure that alternative haplotypes
570 would have the best chance of being split apart. To construct chromosomes for each
571 library, exons from the *S. viridis* gene set reference (v2.1; number of genes = 38,334;
572 number of exons = 289,357) were aligned to each Meraculous assembly (blastn,
573 word_size = 32), and exon alignments with identity >=90% and coverage >=85% were
574 retained. Scaffolds were joined into gene-based scaffolds based on exon alignments;
575 synteny and exon alignments were then used to order and orient the sequences into
576 chromosomes (Figure S11).

577

578 **SNP calling**

579 Reads from the diversity samples were mapped to *S. viridis* v2.1 using bwa-mem[78]. The
580 bam was filtered for duplicates using picard (http://broadinstitute.github.io/picard), and
581 realigned around indels using GATK[71]. Multi sample SNP calling was done using
582 SAMtools mpileup[79] and Varscan V2.4.0[80] with a minimum coverage of eight and a
583 minimum alternate allele frequency of four. An allele is confirmed to be homozygous or

584 heterozygous using a binomial test for significance at a p-value of 0.05. Repeat content
585 of the genome was masked using 24bp kmers. Kmers that occur at a high frequency, up
586 to 5%, were masked. SNP around 25bp of the mask were removed for further analysis.
587 A SNP was included for further analysis if it had a coverage in 90% of the samples, and
588 a MAF > 0.01. Imputation and phasing were done in Beagle V4.0[81]. SNP Annotation
589 was performed using snpEff[82].
590
591 **Pan-genome and PAV analysis**
592 To assess presence/absence variation (PAV) of genes across the diversity panel,
593 admixed individuals were removed from the analysis, leaving 382 individuals (Q>=0.7).
594 We expected that some genes present in wild accessions of *S. viridis* (i.e. the pan-
595 genome) would be either missing or not annotated in the v2.1 reference gene set. To
596 capture these, we included not only proteins from *S. viridis* (v2.1 gene set) but also non-
597 orthologous proteins from *Setaria italica* (v2.2), *Z. mays* (v.PH207) and *S.bicolor*
598 (v3.1)(based on InParanoid comparisons[83]) and aligned these to chromosome
599 integrated assemblies from each of the four subpopulations using blat (-noHead -
600 extendThroughN -q=prot -t=dnax).
601 Genes from *S. viridis* and *S. italica* were considered present if they aligned with
602 greater than 85% coverage and identity, or at least 90% coverage and identity if the
603 exons were broken up and located on no more than three contigs. *Sorghum bicolor* and
604 *Zea mays* genes were considered present if they aligned with greater than 70% identity
605 and 75% coverage (to allow for greater divergence among sequences), or at least 80%
606 identify and coverage if the exons were broken up and located on no more than three

607 contigs. Libraries with fewer than 39,000 genes considered present were excluded as
608 genes were likely lost due to low coverage/poor assembly, with 302 individuals
609 remaining for analysis. 67,079 genes were aligned to each assembly. After removing
610 genes that aligned poorly or not at all to any assembly, a total of 51,323 genes was
611 retained. The resultant PAV matrix (Table S15) was used to determine and cluster
612 genes into their pan-genome designation (core, shell, cloud)[74-76], using discriminant
613 function analysis of principal components (DAPC)[41]. Using successive Kmeans
614 clustering, three distinct clusters (based on BIC criteria) were discovered based on their
615 PAV observance across non-admixed individuals, designated core, shell and cloud.
616 Genomic coordinates for non-orthologous proteins in the pan-genome were determined
617 using the GENESPACE pipeline[74].

618 To discover which genes were over or under represented within each
619 subpopulation based on their expected observance, a $X^2$- test (with Benjamini-
620 Hochberg correction) was performed for each gene among each of the four
621 subpopulations. Significantly over-represented genes (allowing overlap among
622 subpopulations; $p<0.05$) within subpopulations were also tested.

623 To infer syntenic regions when placing non-orthologous genes of interest back on
624 the *S. viridis* genome, we applied the GENESPACE pipeline[74] to the *S. viridis* genome
625 described herein and five other grasses: *S. italica* (v2.2), *S. bicolor* (v3.1), *O. sativa*
626 ('Kitaake', v3.1), *Z. mays* ('Ensemble-18') and *B. distachyon* (v3.1). Genome
627 annotations and assemblies were downloaded from phytozome
628 (phytozome.jgi.doe.gov). In short, GENESPACE runs the following pipeline. First it
629 parses blast results to the top n (default = 1 * (ploidy / 2)) hits for each gene. A separate

630 orthofinder run is conducted for each pairwise combination of genomes; only blast hits
631 within orthogroups are retained. Syntenic blocks are formed with MCScanX[84] with the
632 block size (-s) and gap (-m) parameters set to 25 and 50 respectively. Blocks are culled
633 to those with high mapping density through 2-dimensional nearest neighbor clustering
634 implemented in the R package dbscan[85]. The resulting pruned collinear blast hits are
635 used as anchors for fixed radius nearest neighbor search based on gene rank. All blast
636 hits within the radius (default r = 100 genes) are considered syntenic. Syntenic blast
637 from all species comparisons are fed into a final orthofinder run and parsed into
638 orthologs and paralogs. Plotting routines are implemented in base R.
639
640 **Structural Variants**
641 To detect structural variants within the pan-genome, pseudo PacBio reads were
642 generated from assemblies of non-admixed individuals. Pseudo-reads (length: 10kb;
643 depth 5X) were generated from all contigs greater than 10Kb from each pan-genome
644 assembly. The pseudo-reads were aligned to the *S. viridis* reference genome using
645 nglmr (v0.2.7)[86] with default settings for Pacbio reads. The resulting bam file was sorted
646 using samtools (v1.10) and used for calling structural variants with sniffles (v1.0.11).
647 The structural variant types considered across the pan-genome were: insertions,
648 deletions, and inversions. The average number of SV's detected per library was
649 15,593. A presence/absence matrix for each SV type and was clustered using iterative
650 Kmeans and BIC to determine goodness of fit and the optimal number of clusters
651 present. Based on the BIC criterion, there were three main clusters within the PAV
652 matrix, the first being likely false positives (mean observance 2.8%; n=163,199). The

653 second and third clusters were combined (mean observance 33%; n=33,350) and were
654 used to calculate a distance matrix (method-jaccard) for visualizing subpopulation
655 differences on a PCA plot (Figure 2e).
656
657 **Population structure**
658 Population structure for both SNP and PAV data was estimated using fastStructure[41]
659 and Admixture[42]. SNP markers were randomly subsetted to 50k by LD pruning
660 (parameters: --indep-pairwise 50 50 0.5) in plink 1.9[87], while shell genes (as determined
661 by DAPC clustering) were extracted from the pan-genome. In both analyses, a single
662 sample with a maximum membership coefficient (qi) of <0.7 was considered admixed.
663 Only non-admixed samples from the SNP analysis were used for further analysis. For
664 SNP markers, multidimensional scaling (MDS), identity by state (IBS), and LD estimates
665 (parameters: --r2 --ld-window-kb 500 --ld-window-r2 0) were performed in plink 1.9.
666
667 **Extraction of GBS markers from diversity panel assemblies**
668 To integrate previously published GBS data[67] with our new sequencing data, we
669 extracted the relevant GBS markers from the assembled genomes. The paired end
670 sequences were demultiplexed with the sabre package
671 (https://github.com/najoshi/sabre). Samples were aligned to the reference using bwa-
672 mem and SNP were further called using Varscan 2.3.9 (minimum depth of three and
673 variant allele depth of two). SNP with more than 20% missing data in the GBS data
674 were removed, and then those remaining were merged with the diversity panel (598
675 samples with 8.58M markers). A common set of 55,360 SNP was obtained.

676

677 **LD Decay**

678 The extent of LD for the population was determined as described by[88]. For this, first we
679 extracted one SNP every 100bp using plink (--bp-space 100), and selected a random
680 set of 200,000 markers. LD ($r^2$) was calculated using plink (--ld-window 500 --ld-window-
681 kb 2000). The $r^2$ value was averaged every 100bp of distance. A nonlinear model was fit
682 for this data in R, and the extent was determined as when the LD ($r^2$) nonlinear curve
683 reaches 0.2. Average LD was 100 Kbp. This distance defined the window size for
684 searching for candidate genes in the GWAS analyses.

685

686 **Search for *copia* elements**

687 The *copia38* sequence (6.7 kb) was extracted from the genomic sequence of
688 Seita.5G087200 using repbase (https://www.girinst.org/repbase/). Both the *copia38*
689 sequence and *SvLes1* (Sevir.5G085400) sequence (both genomic sequence and CDS)
690 were aligned to each of the pan-genome assemblies (n=598) using blat (-noHead -
691 extendThroughN). From the blat results, each *copia38* alignment was checked whether
692 it fell within the bounds of the *SvLes1* locus.

693

694 **Environmental correlations**

695 Climate data were obtained from WorldClim[52] using the Raster package in R for each of
696 the 577 samples that have geographical coordinates. Correlations were calculated and
697 visualized using the corrplot R package. To account for correlations between the 19
698 bioclimatic variables, we performed Principal component analysis (PCA) using prcomp

699 in R. The top three principal components that contribute most of the variance were used
700 independently as response variables in the association analysis. GEMMA[89] was used to
701 identify the association of bioclimatic variables and each of the SNP using only kinship
702 in one model and using both kinship and population structure in another model. For
703 population structure estimation, we first LD-pruned the markers in plink (indep-pairwise
704 50 50 0.5) and selected 50000 random markers. PCA was estimated in plink and the
705 top three components were used as covariates in the mixed model to control for
706 population structure. The best model was evaluated using Quantile-Quantile (Q-Q) plots
707 of the observed vs. expected –log10(p) values which should follow a uniform distribution
708 under the null hypothesis. SNP with p-values less than Bonferroni correction were
709 considered significant. Genes within 100Kbp of a significant marker were also
710 considered significant.
711
712 **Signatures of selection and local adaptation:**
713 We employed two statistics for scanning the genome-wide data for signs of positive
714 natural selection: integrated haplotype score (iHS[90]), and Tajima's D[91]. iHS is based on
715 comparing the extended haplotype homozygosity (EHH) score of the ancestral and
716 derived allele of each marker. This test detects loci where natural selection is driving
717 one haplotype to high frequency, leaving recombination little time to break up the
718 linkage group. This was calculated using hapbin[92]. To find genomic regions associated
719 with natural selection, we estimated the fraction of SNP that have |iHS|>2.0 in each
720 100kbp window, with a slide of 10Kbp. The windows with the highest fraction are
721 considered outliers. Tajima's D[91], compares the average number of pairwise differences

722 (π) and the number of segregating sites (S). A negative value indicates positive
723 selection. These values were calculated for 10k windows (with a slide of 10k) and the
724 bottom 1% of the windows were considered outliers.
725
726 **GO and KEGG pathway enrichment analysis**
727 GO enrichment analysis of positively selected genes was performed using topGO[93,94],
728 an R Bioconductor package, to determine overrepresented GO categories across
729 biological process (BP), cellular component (CC) and molecular function (MF) domains.
730 Enrichment of GO terms was tested using Fisher's exact test with $p<0.05$ considered as
731 significant. KEGG[95] pathway enrichment analysis was also performed on those gene
732 sets based on a hypergeometric distribution test and pathways with $p<0.05$ were
733 considered as enriched.
734
735 **GWAS and validation of *SvLes1***
736 The GWAS population to assess seed shattering was planted in the greenhouse
737 facility at Donald Danforth Plant Science Center in April 2014. 215 accessions were
738 chosen from the panel to perform the experiment (Table S8), with four replicates per
739 accession. Shattering phenotype was measured by observing the amount of seed
740 shattering after hand shaking of senesced dry plants. Individual plants were scored
741 using a qualitative scale from 1 to 7. Genotypes were filtered at minor allele frequency >
742 5% for this population. GWAS was performed using a univariate mixed linear model
743 from GEMMA[96], with centered kinship matrix. We used the Wald test p-value[96] for
744 assessing significant peaks, but other p value estimates give similar results. SNP

745 effects were identified using snpEff[82]. Deleterious effects of missense SNPs were
746 predicted using PROVEA [53] on both the reference and alternative allele against the
747 NCBI nr protein database.

748 To knockout *SvLes1* we used the backbone pTRANS_250d as described by
749 Cermák et al.[97]. The protospacer of the guide RNAs targeted the first and second exons
750 of *SvLes1*, upstream of the predicted causal mutation to ensure knock out by frameshift
751 (Figure S12a). The binary vector was introduced into callus tissue using AGL1
752 agrobacterium. Tissue culture and transformation followed an established protocol for *S.*
753 *viridis*[98]. T0 and T1 individuals were genotyped to identify newly acquired mutations
754 near the targeted sites. A T2 homozygote *SvLes1-CRISPR1* was obtained and
755 confirmed by Sanger sequencing, together with homozygotes of the unedited reference
756 line for comparison. To test whether the non-shattering phenotype could be attributed to
757 a single gene, we grew out the T3 seed from two presumptive T2 heterozygotes and
758 several presumptive homozygotes and assessed their genotype at *SvLes1* by PCR and
759 sequencing. Three inflorescences per plant were bagged at heading, and the bags left
760 on until about half the seeds in the panicle appeared mature. Seeds that had fallen off in
761 the bag were collected and weighed. Weights fell largely into two categories, either <35
762 mg, or >195 mg, with only a few weights in between, consistent with the effect of single
763 gene.
764

765 **Germination rate, seed weight, and dispersal distance**

766 Seeds from each genotype were collected, incubated at -80˚C overnight, and then
767 chlorine gas sterilized for 4 hours in a bell jar. Glumes were manually removed, and

768 seeds were sowed onto 0.5X MS with 1% sucrose plates and incubated in the dark at
769 4˚C for two days. Plates were moved into a growth chamber [12 hours light (156
770 μmol•$m^{-2}$•$sec^{-1}$) /12 hours dark, 31˚C days/22 ˚C nights] and percent germination
771 (judged by the emerging radicle tip) was recorded every 24 hours.
772 Seeds were harvested and pooled from five independent plants of each
773 genotype. Five independent replicates of 20 seeds were weighed and recorded.
774 Starting at one week after heading and continuing to maturity, four random plants
775 each from each of two sibling families of *SvLes1-CRISPR1* and wild-type *SvLes1-1*
776 (ME034V) were individually put into a specially designed pot holder in a wind tunnel
777 custom-built for the Kellogg lab with seed collection bins approximately every 10 cm.
778 Blower speed was set to 5 mph for five minutes. Seeds collected in bins at various
779 distances were counted to measure dispersal distance from the parent plant.
780
781 **Tensile strength measurement**
782 Seeds of *SvLes1-1* (ME034v), *SvLes1-2* (A10.1), and *SvLes1-CRISPR1* were
783 treated with 5% liquid smoke overnight at room temperature and kept in wet moss at
784 4°C in the dark for 2-3 weeks. Seeds were sown in Metro mix 360 and grown in a
785 greenhouse with a 14h light/10 h dark cycle, day/night temperatures of 28 and 22°C and
786 relative humidity of 40-50%. Panicles from main stems were collected at 8, 10, 12, 14,
787 16, 18, 20, 24 and 29 days after heading (the apex of the panicles emerged from the
788 leaf sheath). Tensile strength of the spikelet and pedicel junction was measured as
789 described previously[54]. Briefly, panicles were hung upside down from a Mark-10 model
790 M3-2 force gauge. Spikelets were pulled off individually from a panicle using forceps

791 and the peak tension was recorded. Only the most developed spikelets from the central
792 third of the panicle were used to minimize the effects of developmental variation of the
793 spikelets. Six plants with 20 spikelets from each plant were used per genotype per day
794 of measurement. For *SvLes1-1* and *SvLes1-CRISPR1*, the plants in each genotype
795 were offspring of two individual parent plants with the same allele.
796
797 **Histology**
798 Histological procedures followed [99]. Specifically, primary branches were collected
799 from the central third of panicles 12 and 16 days after heading and fixed in FAA (37%
800 formaldehyde: ethanol: $H_2O$: acetic acid = 10:50:35:5), followed by a dehydration series
801 in 50%, 70%, 85%, 95%, 100%, 100% and 100% ethanol and 25%, 50%, 75%, 100%,
802 100% and 100% Histo-Clear (National Diagnostics) series with ethanol as solvent.
803 Paraplast (Leica Biosystems) was then added to each vial of samples and kept
804 overnight, heated at 42°C, and placed in a 60°C oven. The solution was replaced with
805 molten Paraplast twice a day for 3 days. Samples were then embedded in paraffin using
806 a Leica EG1150 tissue embedder, sectioned in 10 μm serial slices with a Leica RM2255
807 automated microtome, and mounted on microscope slides at 42°C on a Premiere XH-
808 2001 Slide Warmer. Sections were then deparaffinized, rehydrated, stained with 0.05%
809 (w/v) toluidine blue O for 1.5 min, and then rinsed with water, dehydrated in ethanol,
810 cleared with xylene and mounted with Permount Mounting Medium (Electron
811 Microscopy Sciences)[36]. Images were taken using a Leica DM750 LED Biological
812 microscope with ICC50 camera module and Leica Acquire v2.0 software.
813

814 **Domestication selective sweep**

815 Raw sequencing reads of foxtail millet lines were obtained from a previous
816 study[59]. Because the average sequencing coverage in the earlier study (~0.5X) is much
817 lower than in our study, we chose 79 lines (Table S16) that have an estimated coverage
818 > 1X to maximize overlapping SNPs and perform analysis. Briefly, *S. italica* sequences
819 were quality trimmed using sickle[100], and aligned with bwa-mem to our *S. viridis* A10.1
820 genome. Multi-sample SNP calling was performed using samtools and Varscan with a
821 minimum depth of 3. For *S.viridis*, the imputed, phased vcf was used for calculation of
822 π, which uses high coverage. π calculation excluded missing samples. Shared SNPs
823 between foxtail millet and *S. viridis* were combined, and missing data were imputed
824 using Beagle 5.0[101]. Nucleotide diversity values $\pi_{viridis}$ and $\pi_{italica}$ were then calculated
825 using vcftools[102] at 100 kb window size. Using genome-wide nucleotide diversity as a
826 reference, we used the program ms[103] to conduct 100,000 coalescent simulations to
827 estimate the variation range of $\pi_{italica}/\pi_{viridis}$ under a domestication bottleneck model for
828 a window of 20 kb. Strength of the bottleneck was determined by genome wide
829 $\pi_{italica}/\pi_{viridis}$. The estimated ranges were then compared to observed values $\pi_{italica}/\pi_{viridis}$
830 to determine significance of domestication selective sweep regions.

831

832 **Retrotransposon insertion in *S. italica Les1***

833 *Copia38* sequence was obtained from the foxtail millet genomic sequence[104]
834 near the ortholog of *SvLes1*, Seita.5G087200 (Si003873m.g). We confirmed the
835 identity of *Copia38* and identified its LTR region by searching its sequence against
836 repbase (https://www.girinst.org/repbase/). We used blastn[105] to identify close homologs

837 of *Copia38* in the Yugu1[104] and A10.1 genomes. RaxML 8.2.9[106] was used to construct
838 the phylogeny of *Copia38* homologs, and pairwise distances of close homologs to
839 *Copia38* were calculated using Kimura 2 parameter model. Read mapping to Yugu1
840 genome follows similar procedures described previously. Paired end reads spanning
841 beyond the left and right junction point of *Copia38* were used to determine if the
842 insertion occurs in an accession or not (Figure S12b).
843
844 **BSA mapping for small leaf angle**
845 The cross between TB159 and A10.1 used pollen of TB159 and follows the protocol
846 described in [107]. F1 individuals were naturally self-pollinated to generate an F2
847 population. 417 F2 individuals were planted and phenotypically scored, and DNA from
848 30 small leaf angle individuals was pooled and sequenced. Sequences are available in
849 the SRA at NCBI, BioProject number PRJNA527194 (to be released after publication).
850 The analysis follows the methods described in a previous BSA study in *S. viridis*[40].
851 Identification of disruptive mutations and missense mutations with deleterious effects
852 follows the same approach described in our GWAS study. Syntenic orthology between
853 *SvLg2* and *liguleless2* in maize was examined and confirmed based on [108].
854
855 **Acknowledgements**
856
857 We thank Zhonghui Wang, Xiaoping Li, and Hui Jiang for their help in maintaining the
858 diversity panel and data collection, Dave Kudrna and Rod Wing at Arizona Genomics

859 Institute for high molecular weight DNA extractions, and members of the Miller Lab at
860 the Danforth Plant Science Center for helpful comments on the manuscript.
861 This work was supported by NSF grants DEB-0115397, MCB-0110809, DEB-0108501,
862 PGRP-0952185, and IOS-1557633 to EAK; and DE-SC0008769 to TPB. The work
863 conducted by the U.S. Department of Energy Joint Genome Institute is supported by the
864 Office of Science of the U.S. Department of Energy under Contract No. DE-AC02-
865 05CH11231.
866

867 **Author contributions**: Credit taxonomy: Conceptualization: IB, TPB, MF, PH, EAK,
868 JS; Methodology: PH, JJenkins, JS; Investigation: CC, KB, MF, AH, PH, JG, JJenkins,
869 JJohnson,TK, JTL, SM, AS, HS, SS, TS, RT, JW, YY; Resources: MF, PH, EAK;
870 Writing - Original Draft: KB, PH, JJ, SM, EAK; Writing - Review & Editing: IB, TPB, MF,
871 PH, EAK, JTL, SM, JS; Visualization: AH, PH, JJ, EAK, JTL; Supervision: IB, TPB,
872 EAK, JS; Project Administration: TPB, EAK, JS; Funding Acquisition: TPB, EAK, JS.
873 Detailed contributions: JS: WGS assembly & sequencing project lead; JJ: map
874 integration, chromosome assembly, analysis; JG: sequencing of BES, QC projects; HS,
875 TK, TS: PacBio sequencing; SS: annotation; MF, PH, EAK: plant collecting; IB, MF, AH,
876 PH, SM: SNP analyses; AH: PAV analyses; JTL: synteny analyses; SM: GWAS of
877 environmental variables; TPB, PH: cloning of *SvLes1*, BSA; PH, EAK, DAN, RT, JW,:
878 phenotyping of *SvLes1*; YY: histology and plant development.
879

880 **Competing interests**: The authors confirm that they have no competing interests.
881

882 **Data availability**: Sequences are available in the SRA at NCBI, BioProject number
883 PRJNA527194 (to be released after publication). Seed stocks for diversity lines are
884 available by contacting co-authors I. Baxter or E. A. Kellogg.
885
886

887 **Literature Cited**


888 1 Grass Phylogeny Working Group. Phylogeny and subfamilial classification of the
889 Poaceae. *Annals of the Missouri Botanical Garden* **88**, 373-457 (2001).
890 2 Kellogg, E. A. *Poaceae*. Pp. 1-416, in K. Kubitzki, ed. *Families and Genera of Vascular*
891 *Plants* (Springer, 2015).
892 3 Soreng, R. J. *et al.* A worldwide phylogenetic classification of the Poaceae (Gramineae)
893 II: An update and a comparison of two 2015 classifications. *Journal of Systematics and*
894 *Evolution* **55**, 259-290, doi:10.1111/jse.12262 (2017).
895 4 Brutnell, T. P. *et al. Setaria viridis*: a model for $C_4$ photosynthesis. *Plant Cell* **22**, 2537-
896 2544 (2010).
897 5 Doust, A. N. & Diao, X.,eds. *The genetics and genomics of Setaria*. Vol. 19 of *Plant*
898 *Genetics and Genomics: Crops and Models* .(Springer International Publishing,
899 Switzerland, 2017).
900 6 Doust, A. N., Kellogg, E. A., Devos, K. M. & Bennetzen, J. L. Foxtail millet, a sequence
901 driven grass model system. *Plant Physiology* **149**, 137-141 (2009).
902 7 Coe, R. A. *et al.* High-throughput chlorophyll fluorescence screening of *Setaria viridis* for
903 mutants with altered $CO_2$ compensation points. *Functional Plant Biology* **45**, 1017-1025
904 (2018).
905 8 Osborn, H. L. *et al.* Effects of reduced carbonic anhydrase activity on $CO_2$ assimilation
906 rates in *Setaria viridis*: a transgenic analysis. *Journal of Experimental Botany* **68**, 299-
907 310 (2017).
908 9 Henry, C. *et al.* Sugar sensing responses to low and high light in leaves of the $C_4$ model
909 grass *Setaria viridis*. *J Exp Bot* **71**, 1039-1052, doi:10.1093/jxb/erz495 (2020).
910 10 Ermakova, M., Lopez-Calcagno, P. E., Raines, C. A., Furbank, R. T. & von Caemmerer,
911 S. Overexpression of the Rieske FeS protein of the Cytochrome b 6 f complex increases

912 $C_4$ photosynthesis in *Setaria viridis*. *Commun Biol* **2**, 314, doi:10.1038/s42003-019-0561-
913 9 (2019).
914 11 Shaw, R. & Cheung, C. Y. M. A mass and charge balanced metabolic model of *Setaria*
915 *viridis* revealed mechanisms of proton balancing in $C_4$ plants. *BMC Bioinformatics* **20**,
916 357, doi:10.1186/s12859-019-2941-z (2019).
917 12 Saha, P. *et al.* Effects of abiotic stress on physiological plasticity and water use of
918 *Setaria viridis* (L.). *Plant Sci* **251**, 128-138, doi:10.1016/j.plantsci.2016.06.011 (2016).
919 13 de Souza, W. R. *et al.* Suppression of a single BAHD gene in *Setaria viridis* causes
920 large, stable decreases in cell wall feruloylation and increases biomass digestibility. *New*
921 *Phytol* **218**, 81-93, doi:10.1111/nph.14970 (2018).
922 14 Martin, A. P. *et al.* A developing *Setaria viridis* internode: an experimental system for the
923 study of biomass generation in a $C_4$ model species. *Biotechnol Biofuels* **9**, 45,
924 doi:10.1186/s13068-016-0457-6 (2016).
925 15 Ferreira, S. S. *et al.* The lignin toolbox of the model grass *Setaria viridis*. *Plant Mol Biol*
926 **101**, 235-255, doi:10.1007/s11103-019-00897-9 (2019).
927 16 Zhu, C., Yang, J., Box, M. S., Kellogg, E. A. & Eveland, A. L. A dynamic co-expression
928 map of early inflorescence development in *Setaria viridis* provides a resource for gene
929 discovery and comparative genomics. *Front Plant Sci* **9**, 1309,
930 doi:10.3389/fpls.2018.01309 (2018).
931 17 Yang, J. *et al.* Brassinosteroids modulate meristem fate and differentiation of unique
932 inflorescence morphology in *Setaria viridis*. *Plant Cell* **30**, 48-66,
933 doi:10.1105/tpc.17.00816 (2018).
934 18 Junqueira, N. E. G. *et al.* Anatomy and ultrastructure of embryonic leaves of the $C_4$
935 species *Setaria viridis*. *Ann Bot* **121**, 1163-1172, doi:10.1093/aob/mcx217 (2018).

936 19 Hunter, C. T. *et al. Setaria viridis* as a model for translational genetic studies of jasmonic
937 acid-related insect defenses in *Zea mays*. *Plant Sci* **291**, 110329,
938 doi:10.1016/j.plantsci.2019.110329 (2020).
939 20 Rodríguez, C. E., Antonielli, L., Mitter, B., Trognitz, F. & Sessitsch, A. Heritability and
940 functional importance of the *Setaria viridis* bacterial seed microbiome. *Phytobiomes* **4**,
941 40-52 (2020).
942 21 Agtuca, B. J. *et al.* In-situ metabolomic analysis of *Setaria viridis* roots colonized by
943 beneficial endophytic bacteria. *Mol Plant Microbe Interact* **33**, 272-283,
944 doi:10.1094/MPMI-06-19-0174-R (2020).
945 22 Ribeiro, A. P. *et al.* Overexpression of BdMATE gene improves aluminum tolerance in
946 *Setaria viridis*. *Frontiers in Plant Science* **8**, doi:10.3389/fpls.2017.00865 (2017).
947 23 Dangol, A., Yaakov, B., Jander, G., Strickler, S. R. & Tzin, V. Characterizing the
948 serotonin biosynthesis pathway upon aphid infestation in *Setaria viridis* leaves. *bioRxiv*
949 https://doi.org/10.1101/642041 (2019).
950 24 Liu, Y. *et al.* A biomimetic *Setaria viridis*-inspired electrode with polyaniline nanowire
951 arrays aligned on MoO3@polypyrrole core–shell nanobelts. *Journal of Materials*
952 *Chemistry A* **6**, 13428-13437, doi:10.1039/C8TA04218G (2018).
953 25 Yu, Y. & Kellogg, E. A. Inflorescence abscission zones in grasses: diversity and genetic
954 regulation. *Annual Plant Reviews* **1**, 1-35, doi:10.1002/9781119312994.apr0619 (2018).
955 26 Fuller, D. Q. Contrasting patterns in crop domestication and domestication rates: recent
956 archaeobotanical insights from the Old World. *Annals of Botany* **100**, 903-924 (2007).
957 27 Harris, D. R. An evolutionary continuum of people-plant interaction, in *Foraging and*
958 *farming: the evolution of plant exploitation* (eds D. R. Harris & G. C. Hillman) 11-26
959 (Routledge, 1989).
960 28 Tanno, K. & Willcox, G. How fast was wild wheat domesticated? *Science* **311**, 1886
961 (2006).

962 29 Hunt, H. V. *et al.* Millets across Eurasia: chronology and context of early records of the
963 genera *Panicum* and *Setaria* from archaeological sites in the Old World. *Vegetation*
964 *History and Archaeobotany* **17 (suppl.)**, S5-S18 (2008).
965 30 Le Thierry d'Ennequin, M., Panaud, O., Toupance, B. & Sarr, A. Assessment of genetic
966 relationships between *Setaria italica* and its wild relative *S. viridis* using AFLP markers.
967 *Theoretical and Applied Genetics* **100**, 1061-1066 (2000).
968 31 Li, Y. & Wu, S. Traditional maintenance and multiplication of foxtail millet (*Setaria italica*
969 (L.) P. Beauv.) landraces in China. *Euphytica* **87**, 33-38 (1996).
970 32 Kuta, D. D., Kwon-Ndung, E., Dachi, S., Ukwungwu, M. & Imolehin, E. D. Potential role
971 of biotechnology tools for genetic improvement of “lost crops of Africa”: the case of fonio
972 (*Digitaria exilis* and *Digitaria iburua*). *African Journal of Biotechnology* **2**, 580-585 (2003).
973 33 Kennard, C., Phillips, L. & Porter, A. Genetic dissection of seed shattering, agronomic,
974 and color traits in American wildrice ( *Zizania palustris* var. *interior* L.) with a comparative
975 map. *Theor Appl Genet* **105**, 1075-1086, doi:10.1007/s00122-002-0988-z (2002).
976 34 Kahler, A. L., Kern, A. J., Porter, R. A. & Phillips, R. L. Maintaining food value of wild rice
977 (*Zizania palustris* L.) using comparative genomics, in *Genomics of Plant Genetic*
978 *Resources* (eds R. Tuberosa, A. Graner, & E. Frison) 233-248 (Springer Science and
979 Business Media, 2013).
980 35 Doust, A. N., Mauro-Herrera, M., Francis, A. & Shand, L. Morphological diversity and
981 genetic regulation of seed dispersal in grasses. *American Journal of Botany* **101**, 1759-
982 1769 (2014).
983 36 Yu, Y., Hu, H., Doust, A. N. & Kellogg, E. A. Divergent gene expression networks
984 underlie morphological diversity of abscission zones in grasses. *New Phytol* **225**, 1799-
985 1815 (2020).
986 37 Waterhouse, R. M. *et al.* BUSCO applications from quality assessments to gene
987 prediction and phylogenomics. *Mol Biol Evol*, doi:10.1093/molbev/msx319 (2017).

988 38 Kellogg, E. A., Aliscioni, S. S., Morrone, O., Pensiero, J. & Zuloaga, F. O. A phylogeny of
989 *Setaria* (Poaceae, Panicoideae, Paniceae) and related genera, based on the chloroplast
990 gene *ndhF*. *International Journal of Plant Sciences* **170**, 117-131 (2009).
991 39 Layton, D. J. & Kellogg, E. A. Morphological, phylogenetic, and ecological diversity of the
992 new model species *Setaria viridis* (Poaceae: Paniceae) and its close relatives. *Amer. J.*
993 *Bot.* **101**, 539-557 (2014).
994 40 Huang, P. *et al. Sparse panicle1* is required for inflorescence development in *Setaria*
995 *viridis* and maize. *Nat Plants* **3**, 17054, doi:10.1038/nplants.2017.54 (2017).
996 41 Raj, A., Stephens, M. & Pritchard, J. K. fastSTRUCTURE: variational inference of
997 population structure in large SNP data sets. *Genetics* **197**, 573-589,
998 doi:10.1534/genetics.114.164350 (2014).
999 42 Alexander, D. H., Novembre, J. & Lange, K. Fast model-based estimation of ancestry in
1000 unrelated individuals. *Genome Res* **19**, 1655-1664, doi:10.1101/gr.094052.109 (2009).
1001 43 Hufford, M. B. *et al.* Comparative population genomics of maize domestication and
1002 improvement. *Nature Genetics* **44**, 808-811 (2012).
1003 44 Shomura, A. *et al.* Deletion in a gene associated with grain size increased yields during
1004 rice domestication. *Nat Genet* **40**, 1023-1028, doi:10.1038/ng.169 (2008).
1005 45 Xu, K. *et al. Sub1A* is an ethylene-response-factor-like gene that confers submergence
1006 tolerance to rice. *Nature* **442**, 705-708, doi:10.1038/nature04920 (2006).
1007 46 Ashikawa, I. *et al.* Two adjacent nucleotide-binding site-leucine-rich repeat class genes
1008 are required to confer Pikm-specific rice blast resistance. *Genetics* **180**, 2267-2276,
1009 doi:10.1534/genetics.108.095034 (2008).
1010 47 Jombart, T. & Ahmed, I. adegenet 1.3-1: new tools for the analysis of genome-wide SNP
1011 data. *Bioinformatics* **27**, 3070-3071, doi:10.1093/bioinformatics/btr521 (2011).

1012 48 Jombart, T., Devillard, S. & Balloux, F. Discriminant analysis of principal components: a
1013 new method for the analysis of genetically structured populations. *BMC Genet* **11**, 94,
1014 doi:10.1186/1471-2156-11-94 (2010).
1015 49 Gordon, S. P. *et al.* Extensive gene content variation in the *Brachypodium distachyon*
1016 pan-genome correlates with population structure. *Nat Commun* **8**, 2184,
1017 doi:10.1038/s41467-017-02292-8 (2017).
1018 50 Feldman, M. J. *et al.* Components of water use efficiency have unique genetic
1019 signatures in the model $C_4$ grass *Setaria*. *Plant Physiol* **178**, 699-715 (2018).
1020 51 Hellmann, H. & Estelle, M. Plant development: regulation by protein degradation.
1021 *Science* **297**, 793-797, doi:10.1126/science.1072831 (2002).
1022 52 Fick, S. E. & Hijmans, R. J. Worldclim 2: New 1-km spatial resolution climate surfaces
1023 for global land areas. *International Journal of Climatology* **37**, 4302-4315 (2017).
1024 53 Choi, Y. & Chan, A. P. PROVEAN web server: a tool to predict the functional effect of
1025 amino acid substitutions and indels. *Bioinformatics* **31**, 2745-2747,
1026 doi:10.1093/bioinformatics/btv195 (2015).
1027 54 Hodge, J. G. & Kellogg, E. A. Abscission zone development in *Setaria viridis* and its
1028 domesticated relative, *Setaria italica*. *Am J Bot* **103**, 998-1005, doi:10.3732/ajb.1500499
1029 (2016).
1030 55 Li, C., Zhou, A. & Sang, T. Rice domestication by reducing shattering. *Science* **311**,
1031 1936-1939 (2006).
1032 56 Konishi, S. *et al.* An SNP caused loss of seed shattering during rice domestication.
1033 *Science* **312**, 1392-1396 (2006).
1034 57 Zhou, Y. *et al.* Genetic control of seed shattering in rice by the APETALA2 transcription
1035 factor *SHATTERING ABORTION1*. *Plant Cell* **24**, 1034-1048 (2012).
1036 58 Lin, Z. *et al.* Parallel domestication of the *Shattering1* genes in cereals. *Nature Genetics*
1037 **44**, 720-724 (2012).

1038 59 Jia, G. *et al.* A haplotype map of genomic variations and genome-wide association
1039 studies of agronomic traits in foxtail millet (*Setaria italica*). *Nat Genet* **45**, 957-961,
1040 doi:10.1038/ng.2673 (2013).
1041 60 Odonkor, S. *et al.* QTL mapping combined with comparative analyses identified
1042 candidate genes for reduced shattering in *Setaria italica*. *Front Plant Sci* **9**, 918,
1043 doi:10.3389/fpls.2018.00918 (2018).
1044 61 Gaut, B. S., Morton, B. R., McCaig, B. C. & Clegg, M. T. Substitution rate comparisons
1045 between grasses and palms: synonymous rate differences at the nuclear gene *Adh*
1046 parallel rate differences at the plastid gene *rbcL*. *Proc Natl Acad Sci U S A* **93**, 10274-
1047 10279 (1996).
1048 62 Pendleton, J. W., Smith, G. E., Winter, S. R. & Johnston, T. J. Field investigations of the
1049 relationships of leaf angle in corn (*Zea mays* L.) to grain yield and apparent
1050 photosynthesis. *Agron. J.* **60**, 422-424 (1968).
1051 63 Tian, F. *et al.* Genome-wide association study of leaf architecture in the maize nested
1052 association mapping population. *Nat Genet* **43**, 159-162, doi:10.1038/ng.746 (2011).
1053 64 Sakamoto, T. *et al.* Erect leaves caused by brassinosteroid deficiency increase biomass
1054 production and grain yield in rice. *Nat Biotechnol* **24**, 105-109, doi:10.1038/nbt1173
1055 (2006).
1056 65 Walsh, J., Waters, C. A. & Freeling, M. The maize gene *liguleless2* encodes a basic
1057 leucine zipper protein involved in the establishment of the leaf blade-sheath boundary.
1058 *Genes Dev* **12**, 208-218, doi:10.1101/gad.12.2.208 (1998).
1059 66 Wang, Z. M., Devos, K. M., Liu, C. J., Wang, R. Q. & Gale, M. D. Construction of RFLP-
1060 based maps of foxtail millet, *Setaria italica* (L.) P. Beauv. *Theor. Appl. Genet.* **96**, 31-36
1061 (1998).
1062 67 Huang, P. *et al.* Population genetics of *Setaria viridis*, a new model system. *Molecular*
1063 *Ecology* **23**, 4192-4295 (2014).

1064 68 Xiao, C. L. *et al.* MECAT: fast mapping, error correction, and de novo assembly for
1065 single-molecule sequencing reads. *Nat Methods* **14**, 1072-1074,
1066 doi:10.1038/nmeth.4432 (2017).
1067 69 Chin, C. S. *et al.* Nonhybrid, finished microbial genome assemblies from long-read
1068 SMRT sequencing data. *Nat Methods* **10**, 563-569, doi:10.1038/nmeth.2474 (2013).
1069 70 Li, H. Aligning sequence reads, clone sequences and assembly contigs with BWA-MEM.
1070 *arXiv* **1303.3997v1 [q-bio.GN]** (2013).
1071 71 McKenna, A. *et al.* The Genome Analysis Toolkit: a MapReduce framework for analyzing
1072 next-generation DNA sequencing data. *Genome Res* **20**, 1297-1303,
1073 doi:10.1101/gr.107524.110 (2010).
1074 72 Kent, W. J. BLAT--the BLAST-like alignment tool. *Genome Res* **12**, 656-664,
1075 doi:10.1101/gr.229202 (2002).
1076 73 Krumsiek, J., Arnold, R. & Rattei, T. Gepard: a rapid and sensitive tool for creating
1077 dotplots on genome scale. *Bioinformatics* **23**, 1026-1028,
1078 doi:10.1093/bioinformatics/btm039 (2007).
1079 74 Lovell, J. T. *et al.* The genomic landscape of molecular responses to natural drought
1080 stress in *Panicum hallii*. *Nat Commun* **9**, 5213, doi:10.1038/s41467-018-07669-x (2018).
1081 75 Haas, B. J. *et al.* Improving the Arabidopsis genome annotation using maximal transcript
1082 alignment assemblies. *Nucleic Acids Res* **31**, 5654-5666, doi:10.1093/nar/gkg770
1083 (2003).
1084 76 Smit, A. F. A., Hubley, R. & Green, P. RepeatMasker Open-3.0. (1996-2011).
1085 77 Chapman, J. A. Meraculous2: fast accurate short-read assembly of large polymorphic
1086 genomes. *arXiv*, 1608.01031 (2016).
1087 78 Li, H. & Durbin, R. Fast and accurate short read alignment with Burrows-Wheeler
1088 transform. *Bioinformatics* **25**, 1754-1760, doi:10.1093/bioinformatics/btp324 (2009).

1089 79 Li, H. *et al.* The Sequence alignment/map format and SAMtools. *Bioinformatics* **25**,
1090 2078-2079 (2009).
1091 80 Koboldt, D. C. *et al.* VarScan 2: somatic mutation and copy number alteration discovery
1092 in cancer by exome sequencing. *Genome Res* **22**, 568-576, doi:10.1101/gr.129684.111
1093 (2012).
1094 81 Browning, S. R. & Browning, B. L. Rapid and accurate haplotype phasing and missing-
1095 data inference for whole-genome association studies by use of localized haplotype
1096 clustering. *Am J Hum Genet* **81**, 1084-1097, doi:10.1086/521987 (2007).
1097 82 Cingolani, P. *et al.* A program for annotating and predicting the effects of single
1098 nucleotide polymorphisms, SnpEff: SNPs in the genome of *Drosophila melanogaster*
1099 strain w1118; iso-2; iso-3. *Fly (Austin)* **6**, 80-92, doi:10.4161/fly.19695 (2012).
1100 83 Sonnhammer, E. L. & Ostlund, G. InParanoid 8: orthology analysis between 273
1101 proteomes, mostly eukaryotic. *Nucleic Acids Res* **43**, D234-239,
1102 doi:10.1093/nar/gku1203 (2015).
1103 84 Wang, Y. *et al.* MCScanX: a toolkit for detection and evolutionary analysis of gene
1104 synteny and collinearity. *Nucleic Acids Res* **40**, e49, doi:10.1093/nar/gkr1293 (2012).
1105 85 Hahsler, M., Piekenbrock, M. & Doran, D. dbscan: fast density-based clustering with R.
1106 *Journal of Statistical Software* **91**, doi: 10.18637/jss.v091.i01 (2019).
1107 86 Sedlazeck, F. J. *et al.* Accurate detection of complex structural variations using single-
1108 molecule sequencing. *Nat Methods* **15**, 461-468, doi:10.1038/s41592-018-0001-7
1109 (2018).
1110 87 Chang, C. C. *et al.* Second-generation PLINK: rising to the challenge of larger and richer
1111 datasets. *Gigascience* **4**, 7, doi:10.1186/s13742-015-0047-8 (2015).
1112 88 Remington, D. L. *et al.* Structure of linkage disequilibrium and phenotypic associations in
1113 the maize genome. *Proc Natl Acad Sci U S A* **98**, 11479-11484,
1114 doi:10.1073/pnas.201394398 (2001).

1115 89 Zhou, X. & Stephens, M. Efficient multivariate linear mixed model algorithms for
1116 genome-wide association studies. *Nat Methods* **11**, 407-409, doi:10.1038/nmeth.2848
1117 (2014).
1118 90 Voight, B. F., Kudaravalli, S., Wen, X. & Pritchard, J. K. A map of recent positive
1119 selection in the human genome. *PLoS Biol* **4**, e72, doi:10.1371/journal.pbio.0040072
1120 (2006).
1121 91 Tajima, F. Statistical method for testing the neutral mutation hypothesis by DNA
1122 polymorphism. *Genetics* **123**, 585-595 (1989).
1123 92 Maclean, C. A., Chue Hong, N. P. & Prendergast, J. G. hapbin: An efficient program for
1124 performing haplotype-based scans for positive selection in large genomic datasets. *Mol*
1125 *Biol Evol* **32**, 3027-3029, doi:10.1093/molbev/msv172 (2015).
1126 93 Alexa, A., Rahnenfuhrer, J. & Lengauer, T. Improved scoring of functional groups from
1127 gene expression data by decorrelating GO graph structure. *Bioinformatics* **22**, 1600-
1128 1607, doi:10.1093/bioinformatics/btl140 (2006).
1129 94 topGO: Enrichment Analysis for Gene Ontology. R package version 2.24.0 v. 2.24.0
1130 (http://bioconductor.org/packages/release/bioc/html/topGO.html, 2016).
1131 95 Kanehisa, M. & Goto, S. KEGG: Kyoto Encyclopedia of Genes and Genomes. *Nucleic*
1132 *Acids Res* **28**, 27-30, doi:10.1093/nar/28.1.27 (2000).
1133 96 Zhou, X. & Stephens, M. Genome-wide efficient mixed-model analysis for association
1134 studies. *Nat Genet* **44**, 821-824, doi:10.1038/ng.2310 (2012).
1135 97 Cermák, T. *et al.* A multipurpose toolkit to enable advanced genome engineering in
1136 plants. *Plant Cell* **29**, 1196-1217, doi:10.1105/tpc.16.00922 (2017).
1137 98 VanEck, J., Swartwood, K., Pidgeon, K. & Maxon-Stein, K. *Agrobacterium tumefaciens*-
1138 mediated transformation of *Setaria viridis*, in *Genetics and genomics of Setaria Plant*
1139 *Genetics and Genomics: Crops and Models* (eds A. Doust & X. Diao) 343-356
1140 (Springer, 2016).

1141 99 Ruzin, S. E. *Plant microtechnique and microscopy*. (Oxford University Press, 1999).
1142 100 A sliding-window, adaptive, quality-based trimming tool for FastQ files (Version 1.33)
1143 Available at https://github.com/najoshi/sickle. (2011).
1144 101 Browning, B. L. & Browning, S. R. Genotype imputation with millions of reference
1145 samples. *Am J Hum Genet* **98**, 116-126, doi:10.1016/j.ajhg.2015.11.020 (2016).
1146 102 Danecek, P. *et al.* The variant call format and VCFtools. *Bioinformatics* **27**, 2156-2158,
1147 doi:10.1093/bioinformatics/btr330 (2011).
1148 103 Hudson, R. R. Generating samples under a Wright-Fisher neutral model of genetic
1149 variation. *Bioinformatics* **18**, 337-338 (2002).
1150 104 Bennetzen, J. L. *et al.* Reference genome sequence of the model plant *Setaria*. *Nature*
1151 *Biotechnology* **30**, 555-561 (2012).
1152 105 Altschul, S. F., Gish, W., Miller, W., Myers, E. W. & Lipman, D. J. Basic local alignment
1153 search tool. *J Mol Biol* **215**, 403-410, doi:10.1016/S0022-2836(05)80360-2 (1990).
1154 106 Stamatakis, A. RAxML version 8: a tool for phylogenetic analysis and post-analysis of
1155 large phylogenies. *Bioinformatics* **30**, 1312-1313, doi:10.1093/bioinformatics/btu033
1156 (2014).
1157 107 Jiang, H., Barbier, H. & Brutnell, T. Methods for performing crosses in *Setaria viridis*, a
1158 new model system for the grasses. *J Vis Exp*, doi:10.3791/50527 (2013).
1159 108 Schnable, J. C., Freeling, M. & Lyons, E. Genome-wide analysis of syntenic gene
1160 deletion in the grasses. *Genome Biology and Evolution* **4**, 265-277 (2012).
1161

1162 **Figure and Table Legends**

1163

1164 **Fig. 1. a** *Setaria viridis*, in its common highly disturbed habitat next to a road. **b**
1165 Average library coverage, contig N50 (Kb), pan-genome assembly size, and number of
1166 genes per library; red vertical line in lower right panel represents the number of genes
1167 necessary for a library to be included for PAV analysis (n=39,000).

1168

1169 **Fig. 2.** PAV and SNP diversity of subpopulations. **a** Geographic distribution and
1170 population assignment of North American accessions based on SNP data. **b**
1171 Geographic distribution and population assignment of Eurasian accessions based on
1172 SNP data. **c** PCA of SNP data, showing placement of North American samples among
1173 Eurasian ones. **d** PCA of PAV variants, excluding admixed individuals. **e** PCA of
1174 structural variants, excluding admixed individuals. Both SNP and PAV data clearly
1175 separate the Central-North population (green) from the others, and the structural
1176 variants distinguish all populations. *, accession is admixed; black rim on circle,
1177 accession is in its native range.

1178

1179 **Fig. 3.** GWAS and cloning of *Les1*. **a** Manhattan plot of GWAS result, red line showing
1180 p=0.01 after Bonferroni correction. **b** Zoom in to peak on Chromosome 5; larger dots
1181 represent missense SNPs identified by snpEff. Different colors of missense SNPs
1182 indicate Provean score range (blue for >-2.5, green for <-2.5 and >-4.1, red for <-4.1; -
1183 2.5 and -4.1 represent 80% and 90% specificity). Lower scores indicate higher
1184 likelihood of deleterious effects of the mutation. **c** Table of *Les1* alleles in *S. viridis* (*Sv*)

1185 and *S. italica* (*Si*), with structural characteristics, background line, and shattering
1186 phenotype. **d** Sanger sequence validating the position of the adenine insertion
1187 (frameshift) in *SvLes1-CRISPR-1*.
1188
1189 **Fig. 4.** Phenotypic characterization of *SvLes1-CRISPR1* mutants and naturally
1190 occurring alleles. **a** Force required to break the AZ (tensile strength in gm of force) in
1191 *SvLes1-1*, *SvLes1-2*, and *SvLes1-CRISPR1* lines, measured every two days starting at
1192 8 days after heading. **b** Image of *S. viridis* high shattering (*SvLes1-1* in ME034), left two
1193 panicles) and *SvLes1-CRISPR1* mutant panicles seven weeks after heading. Both
1194 mutants have retained their seed, unlike ME034 which has shed most of its seed at this
1195 time point. **c** Seed dispersal distances in a wind tunnel, measured from four
1196 independent high shattering plants (*SvLes1-1* in ME034) and eight *SvLes1-CRISPR1*
1197 plants at week 6. Wind speed was 5 mph coming from the left of the diagram. The
1198 plant, indicated by P, was placed in middle of the tunnel; some seed fell on the
1199 windward side (negative distance values) due to oscillation of the plant. Although mean
1200 dispersal distance was approximately the same for both alleles, the *SvLes1-CRISPR1*
1201 plants released significantly fewer seeds at each distance that the *SvLes1-1* plants.
1202
1203 **Fig. 5.** Phenotype and mapping of small leaf angle. **a, b** Small leaf angle phenotype in
1204 TB159. **c** BSA mapping result, red arrow indicating QTL. **d** Synteny analysis around
1205 *SvLg2* and maize *lg2* locus.
1206
1207 **Fig. S1.** Cumulative citations for *Setaria viridis*, 1960-present, from Scopus, accessed

1208 Jan. 2, 2020.

1209

1210 **Fig. S2.** Population distribution and structure of North American accessions.

1211 Population assignment based on SNPs. **a** distribution of all accessions; **b** distribution of

1212 non-admixed samples only; **c** STRUCTURE plot including all accessions.

1213

1214 **Fig. S3.** Over-represented GO categories and KEGG enrichment pathways for each

1215 subpopulation.

1216

1217 **Fig. S4.** Correlations among the bioclim variables[52] for the 577 accessions for which

1218 latitude-longitude information was available.

1219

1220 **Fig. S5.** GWAS results using each of the first three environmental PCs as response

1221 variable. PC1 found no significant loci, PC2 found one, and PC3 found several.

1222

1223 **Fig. S6.** Loci showing significant signatures of selection for each population. Left

1224 column, proportion of SNP with |iHS| >2 for each of the population. Right column,

1225 Tajima's D represented in -ve scale. 100 Kbp windows (slide 10 Kbp). Horizontal lines

1226 represent 95th and 99th percentiles for iHS and 1st and 5th percentiles for Tajima's D.

1227

1228 **Fig. S7. a** Comparison of seed germination rates of *SvLes1-1* and *SvLes1-CRISPR1*

1229 lines. Three plates of Setaria seed with n≥ 53 were measured for germination and

1230 averaged. Error is standard deviation. **b**, Comparison of seed weight of *SvLes1-1* and

1231 *SvLes1-CRISPR1* lines. Twenty seed weight was measured from 5 independent plants.
1232 *SvLes1-CRISPR1* seeds weighed significantly less ($p<0.0001$), but this did not affect
1233 germination.
1234
1235 **Fig. S8.** *SvLes1-2* (A10.1), *SvLes1-1*, and *SvLes1-CRISPR1* have similar anatomical
1236 structures in the abscission zone. Spikelets from main panicles 12 days after heading,
1237 stained with 0.05% Toluidine blue O. **a,b** *SvLes1-2* (A10.1). **c,d** *SvLes1-1.* **e,f** *SvLes1-*
1238 *CRISPR1.* **a,c,e** Scale bars = 100 µm. **b,d,f** Scale bars **=** 20 µm. En, endosperm; em,
1239 embryo. White dotted line, approximate position of AZ.
1240
1241 **Fig. S9.** Phylogenetic tree of *Copia38* copies in A10.1 and Yugu1 genomes. Red clade
1242 shows the recent explosion that contains the copy inserted into *SiLES1*. Gene models in
1243 green, *S. italica*; in blue, *S. viridis*.
1244
1245 **Fig. S10.** Representative dot plots**. a** Dot plot of clone 114809 on a region of scaffold_1.
1246 This alignment is representative of the high quality clone alignments in 239 of the 365
1247 available clones. **b** Dot plot of clone 113526 on a region of scaffold_3, which is
1248 representative of the 36 clones that landed in repetitive regions of the genome.
1249
1250 **Fig. S11.** Plots of marker placements for each of the 9 chromosomes (scaffolds) of *S.*
1251 *viridis*.
1252
1253 **Fig. S12.** **a** guide RNA protospacers and their position relative to allelic mutations and

1254 gene model. **b** Method used to detect *Copia38* insertion.

1255

1256 **Table S1.** Metadata for 598 diversity lines. LIB, library; Q4 max, membership
1257 coefficient obtained from the output of STRUCTURE; Q4_subpop, subpopulation
1258 assignment using SNP data; Name, collector's name and number or other unique
1259 identifier; new name, name in germplasm collection, lat, latitude of original collection;
1260 long, longitude of original collection. Subpopulation assignments correspond to those in
1261 figures, viz. Magenta -Central - 95 samples; Orange - West coast - 222 samples; Green
1262 – Central-North - 148 samples; blue - Central-East - 133 samples. bio1-bio19 are
1263 values of environmental variables from the WorldClim database [52]. SRA is the
1264 accession number for the Sequence Read Archive at the NCBI.

1265

1266 **Table S2**. Subpopulation statistics. Numbers of non-admixed individuals based on SNP
1267 analysis; numbers used for each subpopulation in the PAV analysis are lower because
1268 not all libraries assembled well enough to be used. Number of over-represented genes
1269 is the number significant for that subpopulation alone. SNP, single nucleotide
1270 polymorphism; Pi/bp, polymorphisms per basepair; IBD, identity by descent for the
1271 subpopulation; IBS, identity by state for the subpopulation; LD, linkage disequilibrium;
1272 LD $R^2$>=0.7%, percent of pairwise comparisons with LD>=0.7.

1273

1274 **Table S3** PAV diversity by subpopulation, listing over- and under-represented loci.

1275

1276 **Table S4**. Loadings of bioclim variables on the first three principal components. PC,

1277 principal component; min, minimum; max, maximum.

1278

1279 **Table S5.** Annotation of genes containing markers significantly associated with

1280 environmental variables.

1281

1282 **Table S6.** Significant Biological process GO terms for environmental associations.

1283

1284 **Table S7.** GO terms and KEGG pathways enriched for loci under selection, as identified

1285 by Tajima's D and the absolute value of iHS.

1286

1287 **Table S8.** *Setaria viridis* samples scored for shattering phenotype. LIB, library number;

1288 Name, original accession identified; New_name, internal Brutnell lab identifier;

1289 Population, population assignment; Score_lowShatter, shattering index; Allele,

1290 nucleotide at position Chr_05:6849363.

1291

1292 **Table S9.** Comparison of pairwise diversity in the region surrounding *SiLes1* vs.

1293 *SvLes1*. Diversity is significantly lower in the *Les1* region in *S. italica* than in *S. viridis*,

1294 *p*=0.0066 based on 100,000 coalescent simulations. Description, interval considered for

1295 diversity estimates; total, total number of bp, centered on the gene; either side, number

1296 of bp upstream and downstream of the gene.

1297

1298 **Table S10.** Comparison of linkage disequilibrium (LD) in the region surrounding *SiLes1*

1299 vs. *SvLes1*. Intervals as in Table S9.

1300

1301 **Table S11.** Genomic libraries included in the *Setaria viridis* genome assembly and their

1302 respective assembled sequence coverage levels in the final release.

1303 *Average read length of PACBIO reads.

1304

1305 **Table S12.** PACBIO library statistics for the libraries included in the *Setaria viridis*

1306 genome assembly and their respective assembled sequence coverage levels.

1307

1308 **Table S13.** Summary statistics of the initial output of the QUIVER polished MECAT

1309 assembly. The table shows total contigs and total assembled base pairs for each set of

1310 scaffolds greater than the size listed in the left hand column.

1311

1312 **Table S14.** Final summary assembly statistics for chromosome scale assembly. Final

1313 summary assembly statistics for chromosome scale assembly. Scaffold sequence total

1314 is all bases in the release plus gaps. Chromosome sequence is all bases in the

1315 chromosomes not including gaps. Total bases is all bases in the release excluding

1316 gaps.

1317

1318 **Table S15**. PAV matrix for all non-admixed individuals.

1319

1320 **Table S16.** *Setaria italica* lines used for π *italica* - π *viridis* comparison and for test of

1321 selective sweeps. Data from [59], downloaded from the Sequence Read Archive at NCBI.

1322